PRESYNAPTIC PLASTICITY AT AGEING AUDITORY RIBBON SYNAPSES: ENLARGED SYNAPTIC RIBBONS WITH INCREASED Ca^{2+} MICRODOMAINS AND REDUCED BK CHANNEL CLUSTERS

Abbreviated title: Synaptopathy at aging auditory ribbon synapses

Thibault PEINEAU[1,2#], Séverin BELLEUDY[1#], Yohan BOULEAU[1,2] and Didier DULON[1,2*]

[1]Neurophysiologie de la Synapse Auditive, INSERM UMRS 1120, Bordeaux Neurocampus, Université de Bordeaux, 33076 Bordeaux, France

[2] Institut de l'Audition, Centre Institut Pasteur/Inserm, 63 rue de Charenton, 75012 Paris

[*] Corresponding author: didier.dulon@inserm.fr

# First co-authors, contributed equally to the study

Key words: Deafness, aging, auditory hair cells, synaptic ribbons, auditory synaptopathies

Conflict of Interest

The authors declare that the research was conducted in the absence of any commercial or financial relationships that could be construed as a potential conflict of interest.

Author Contributions

DD designed research; SB, TP, YB performed research and analyzed the data. DD wrote the paper.

Funding & acknowledgments

This work was supported by a grant from the Fondation Pour l'Audition and from the french society of audioprosthesis professionals, Entendre SAS (Saint Cyr l'Ecole 78210 France).

ABSTRACT

Cochlear inner hair cells (IHCs) harbor a peculiar presynaptic organelle, the ribbon, which is essential for aggregating synaptic vesicles and organizing Ca^{2+} channels at the active zone. Emerging evidence suggests that damage to the ribbon synapses represents an important form of cochlear synaptopathy that seems prevalent in age-related sensorineural hearing loss. The functional changes occurring at these synapses during aging are not fully understood. Here, we characterized the age-related changes in IHCs of C57BL/6J mice, a strain which is known to carry a cadherin23 mutation and experiences early hearing loss with age. We found a progressive loss of synaptic ribbons with aging, starting before postnatal day 180 (P180) and reaching up to 50 % loss in middle age mice at P365. A deletion of the *Otof* gene, encoding the Ca^{2+} sensor otoferlin produced an accelerated loss of IHC ribbons with aging, with a 50 % loss by P60. In both *Otof* $^{+/+}$ and *Otof* $^{-/-}$ C57BL/6J mice, the synaptic ribbons became larger with aging and IHCs displayed a drastic cell surface reduction with a large decrease in extrasynaptic BK-channel expression. These changes are indicative of oxidative stress and synaptic autophagy as suggested by an increased expression of the autophagosomal protein LC3B. Furthermore, whole-cell patch-clamp recordings and calcium imaging in IHCs from old *Otof* $^{+/+}$ P365 C57BL/6J mice indicated an increase in Ca^{2+}-channel density and a stronger exocytosis at the remaining ribbon active zones, suggesting synaptic release potentiation possibly explaining hyperacusis and recruitment in the elderly.

SIGNIFICANCE STATEMENT

Age-related hidden hearing loss is often described as a cochlear synaptopathy that results from a progressive degeneration of the ribbon synapses contacting the inner hair cells (IHCs). We show that the auditory defect of aging C57BL/6J mice is associated with a large shrinkage of IHCs and a drastic enlargement of their remaining presynaptic ribbons. Synaptic Ca^{2+} microdomains and exocytosis were largely increased in old IHCs, while on the contrary the expression of the fast repolarizing BK channels, known to negatively control transmitter release, was decreased. This age-related synaptic plasticity in IHCs suggested a functional potentiation of synaptic transmission at the surviving synapses, a process that could partially compensate the decrease in synapse number and underlie hyperacusis.

INTRODUCTION

Age-related hearing loss (ARHL or presbycusis) is the most prevalent form of sensory disability in human populations and adversely affects the quality of life of many elderly individuals. The development of ARHL has been generally considered to be associated with primary degeneration of cochlear hair cells, with secondary deafferentation associating degeneration of spiral ganglion neurons and ribbon synapses. However, recent studies have resulted in a paradigm shift in the understanding of the early cause of ARHL (Kujawa and Liberman, 2015; 2019). During aging, hearing thresholds in the elderly often remain normal but speech intelligibility become hampered, especially in noisy environment. This pathology in the elderly is referred as hidden hearing loss and has been proposed to be caused by an early loss of ribbon synapses contacting the inner hair cells (IHCs), well before any major loss of hair cells and spiral ganglion neurons (Stamataki et al., 2006). While glutamate excitotoxicity, resulting in nerve terminal swelling, has been proposed to play a role in the setting of noise-induced hearing loss (Pujol and Puel, 1999; Hu et al., 2020), the molecular mechanisms underlying the degeneration of the cochlear ribbon synapses during aging remain to be elucidated. Oxidative damage due to an increase in ROS levels seems to plays a crucial role in ARHL (Fu et al., 2018) but how the ribbon synapses are functionally affected remain unknown.

The C57BL/6J inbred strain of mice has been extensively studied and used as model for ARHL (Johnson et al., 1997; Spongr et al., 1997; Hequembourg and Liberman, 2001; Bartolome et al., 2002; Henry, 2002). This mouse strain carries a cadherin23 mutation (*Cdh23* ^{753A}, also known as *Ahl*), which affects inner ear structures, characterized by progressive degeneration of ribbon synapses and spiral ganglion neurons, and results in age-related hearing loss. *Ahl* is a recessive single nucleotide mutation at 753 (G=>A) on the *Cdh23* gene on mouse chromosome 10 (Noben-Trauth et al., 2003). The *Ahl* mutation is the first mutation discovered in association with ARHL and appears to be the most common ARHL mutation in mice (Johnson et al., 1997; Noben-Trauth et al., 2003). In C57BL/6J mice, auditory sensitivity declines at significantly faster rates than gravity receptor sensitivity (Mock et al., 2016). *Cdh23* encodes cadherin 23, a protein necessary for inner ear development and maintenance of the sensory hair cell structures, in particular the tip and lateral links of the stereocilia at the hair bundle (Siemens et al., 2004; Söllner et al., 2004; Kazmierczak et al., 2007; Michel et al., 2005; Lagziel et al., 2005), but growing anatomical evidence also suggests that synaptic

rearrangements on sensory hair cells also contribute to auditory functional decline in C57BL/6J mice (Stamataki et al., 2006; Zachary and Fuchs, 2015; Jiang et al., 2015). Remarkably, an even earlier degeneration of auditory ribbon synapses has been reported in C57BL/6J mice when the otoferlin gene is lacking (*Otof* $^{-/-}$ mice) (Roux et al., 2006; Vincent et al., 2017; Tertrais et al., 2019). We recall that otoferlin is a crucial Ca^{2+} sensor that controls synaptic vesicle exocytosis at auditory inner hair cell (IHC) ribbon synapses (Beurg et al, 2010; Michalski et al., 2017) and vestibular hair cell synapses (Dulon et al., 2009). The role of otoferlin in the development and maintenance of the synaptic ribbons is not known. The present study aimed to decipher the role of cadherin 23 and otoferlin in age-related dysfunction and degeneration of the IHC synapses in C57BL/6J mice bearing the *Ah1*-mutation only and in mice lacking, in addition, the otoferlin gene. Our study will characterize the morphological and functional changes occurring at the IHC synaptic ribbons of aged C57BL/6J mice. We will show that aging-associated changes in the IHC ribbon synapses also occurred in silent synapses lacking otoferlin, suggesting that the degenerative synaptic process is independent of an exacerbated glutamate excitotoxicity.

METHODS

Mice

Inbred C57BL/6J mice, which are homozygous for the recessive cadherin23 mutation *Cdh23*^{753A} (also known as Ah1), and inbred transgenic C57BL/6J ice carrying a deletion of the *Otof* gene (*Otof* $^{-/-}$; Roux et al., 2006) were used in the present study. Hearing thresholds and IHC ribbon counts in mice of either sex were performed at postnatal ages: P15, P30, P60, P180 and P365. CBA/J mice (from Charles River) were also tested as controls at P50, P250 and P360. Animal care and all procedures were approved by the institutional care and use committee of the University of Bordeaux and the French Ministry of Agriculture (agreement C33-063-075).

Assessment of hearing thresholds (ABRs)

To record ABRs (Auditory Brainstem Responses, which represent the sound-evoked synchronous firing of the auditory cochlear nerve fibers and the central auditory relays), mice were anesthetized with intraperitoneal injection of xylazine (6 mg/ml, Rompun Bayer) and ketamine (80 mg/ml, Virbac) mixture diluted in physiological saline. The mouse was placed in a closed acoustic chamber and its body temperature was kept constant at 37°C during ABRs recording. For sound stimulus generation and data acquisition, we used a TDT RZ6/BioSigRZ system (Tucker-Davis Technologies). Click-based ABR signals were averaged after the presentation of a series of 512 stimulations. Thresholds were defined as the lowest stimulus for recognizable wave-I and II. The amplitude of ABR wave-I was estimated by measuring the voltage difference between the positive (P1) and negative (N1) peak of wave-I. Sound intensities of 10 to 90 dB SPL in 10 dB step, were tested.

Distortion product otoacoustic emissions (DPOAEs), which originate from the electromechanical activity of the outer hair cells (OHCs), were tested by using two simultaneous continuous pure tones with frequency ratio of 1.2 (f1 = 12.73 kHz and f2 = 15,26 kHz). DPOAEs were collected with the TDT RZ6/BioSigRZ system designed to measure the level of the "cubic difference tone" 2f1-f2.

Tissue preparation and imunocytochemistry

Mice were deeply anesthetized with isofluorane (Vetflurane, Virbac). The ramps of the cochlear apparatus were dissected and prepared as previously described by Vincent et al.

(2014). Inner ears (cochleae) were fixed by incubation in 4% paraformaldehyde in phosphate-buffered saline (PBS), pH 7.4, at 4°C overnight and washed with cold phosphate buffered saline (PBS). They were then incubated for 2 days in PBS solution containing 10% EDTA pH 7.4 at 4°C. The middle part of the organ of Corti (area encoding between 8 and 16 kHz) was then dissected and the tectorial membrane removed. The tissue was first incubated with PBS containing 30% normal horse serum and triton X100 0.5 % for 1 hour at room temperature. Synaptic ribbons were labeled with anti-CtBP2 (1/200 Goat polyclonal, Santa Cruz, USA ; cat # SC-5966 or 1/200 Mouse IgG1 monoclonal antibody BD Biosciences, cat # 612044). Otoferlin was labeled with a mouse monoclonal antibody (1/200 AbCam, cat # ab53233). VGLUT3 was labeled with a Mouse monoclonal antibody (1/400, Synaptic System, cat # 135211). Autophagy was detected by labeling LC3B protein with anti Rabbit monoclonal antibody (1/200 LC3B(D11) XP, Cell Signaling Technology, cat # 3868). BK channels were labeled with a Rabbit polyclonal antibody (1/200, Alomone, Israel, cat #APC-021. Explants of Organ of Corti were incubated overnight at 4°C with primary antibodies. The following fluorescent secondary antibodies 1/500 were then used: anti-Goat Donkey polyclonal Fluoprobes 547H (Interchim, cat# FP-SB2110) , anti-Mouse Donkey polyclonal Fluoprobes 647H (Interchim, cat# FP-SC4110), anti-Mouse Donkey polyclonal Alexa Fluor 488 (AbCam, cat# ab150109), anti-Mouse Goat polyclonal Alexa Fluor 546 (Molecular Probes, cat# A-11003), anti-Mouse Goat polyclonal Alexa Fluor 488 (Molecular Probes, cat# A-10680), anti-Rabbit Donkey polyclonal Fluoprobes 594 (Interchim, cat# FP-SD5110). Actin-F was also used to visualize hair cells (1/100, Phalloidin Fluoprobe 405, Interchim, Montlucon, France; cat # FP-CA9870). For Image Acquisition, organ of Corti samples were analyzed using a confocal laser scanning microscope Leica SP8 with a 63X oil immersion objective (NA = 1.4) and white light laser (470 to 670 nm) (Bordeaux Imaging Center). Phalloidin was imaged by using a diode laser at 405 nm also mounted on the microscope. Stack images were acquired with the same parameters as previously described (Vincent et al, 2014). Image analysis was performed with ImageJ software. Inter-ribbon distance (center mass distance) was calculated using the colocalisation JACoP plugin of ImageJ (Bolte and Cordelières, 2006) in at least 20 IHCs per age and genotype.

High resolution imaging of synaptic ribbons with confocal STED microscopy

For high-resolution imaging of IHC ribbons, we used a Leica DMI6000 TCS SP8 STED microscope with 93X glycerol immersion objective (NA 1.3) (Bordeaux Imaging Center).

Mouse sensory organs were fixed and incubated with primary anti CtBP2 (1/100) antibodies in conditions similar to those described above for confocal microscopy. Secondary antibodies Goat anti- IgG1 Mouse polyclonal Alexa Fluor 647 (Jackson, cat# 115-605-205) were used to label CtBP2 primary antibodies. The pulsed STED depletion laser (pulsed laser IR, Spectra Physics Mai Tai) was set at 775 nm. Stack images were acquired with the following parameters: scan rate 200 Hz, 775 nm depletion laser power between 8 and 15%, scans frames accumulated per *X*-*Y* section 8 times, z- step size 0.25 µm, number of plans between 8 and 10, pixel size 20 nm giving an *X*-*Y* image size of 21 × 5 µm (1024 × 256 pixels).

Counting spiral ganglion neurons and nerve fibers

The afferent nerve fibers of the auditory nerve were fluorescently labeled using a retrograde track tracing technique with dextran amines (Fritzsch et al., 2016). Cochleae were extracted from temporal bone of freshly euthanised mice and rapidly immerged intact into cold artificial perilymph (NaCl 135; KCl 5.8; $CaCl_2$ 1.3; $MgCl_2$ 0.9; NaH_2PO_4 0.7; Glucose 5.6; Na pyruvate 2; HEPES 10, pH 7.4, 305 mOsm). A small crystal of tetramethylrhodamine dextran amines 3000 (Life technologies, NY) was placed for 15-20 min at the edge of the auditory nerve coming out at the internal auditory canal of the intact cochlea. The intracochlear sensory tissues were then fixed by gentle perfusion of a 4% PFA solution for 30 min and rinse with artificial perilymph. They were then decalcified for 2 days in PBS solution containing 10% EDTA pH 7.4 at 4°C. The cochleae were then sliced with a razor blade along the longitudinal cochlear axes and the slices were then mounted on a glass-slide for fluorescent confocal microscopy observation. The quantification of the spiral ganglion neurons per surface area of the neural ganglion were made in the middle part of the cochlea in a region encoding 8-16 kHz, by using the 3D object counter application of ImageJ software.

Ca^{2+} currents and whole-cell membrane capacitance measurement in IHCs

Measurements of resting membrane capacitance of IHCs were performed at P18-P21 in the 20-40% normalized distance from the apex, an area coding for frequencies ranging from 8 to 16 kHz, by using an EPC10 amplifier controlled by Patchmaster pulse software (HEKA Elektronik, Germany), as previously described in detail (Vincent et al., 2015). The organ of Corti was incubated in an extracellular perilymph-like solution containing NaCl 135; KCl 5.8; $CaCl_2$ 5; $MgCl_2$ 0.9; NaH_2PO_4 0.7; Glucose 5.6; Na pyruvate 2; HEPES 10, pH 7.4, 305 mOsm. This extracellular solution was complemented with 0.25 µM of apamin (Latoxan; cat

L8407) and 1 µM of XE-991 (Tocris Bioscience; cat # 2000) to block SK channels and KCNQ4 channels, respectively. The external Ca^{2+} concentration was increased from 1.3 to 5 mM to enhance the amplitude of Ca^{2+} currents to levels nearby body temperature. All experiments were performed at room temperature (22°C–24°C)

Patch pipettes were pulled with a micropipette Puller P-97 Flaming/Brown (Sutter Instrument, Novato, CA, USA) and fire-polished with a Micro forge MF-830, (Narishige, Japan) to obtain a resistance range from 3 to 5 MΩ. Patch pipettes were filled with a cesium-based intracellular solution containing (in mM): CsCl 145; $MgCl_2$ 1; HEPES 5; EGTA 1; TEA 20, ATP 2, GTP 0.3, pH 7.2, 300 mOsm. Measurements of the resting membrane capacitance (cell size) of IHCs were obtained in whole-cell voltage-clamp configuration at -70 mV and after 2 min equilibrium of the internal patch-pipette recording solution with the IHC cytosol.

Intracellular Ca^{2+} imaging

Fluorescent Ca^{2+} signals were measured with a C2 confocal system and NIS-element imaging software (Nikon) coupled to the FN1 upright microscope as previously described (Vincent et al., 2014 ; 2017). For Ca^{2+} imaging in IHCs, in which membrane capacitance and Ca^{2+} currents were simultaneously recorded, patch pipettes were filled with the same cesium-base solution described above supplemented with 50 µM of the red fluorescent indicator Rhod2 (R14220, Invitrogen™, Thermofisher Scientific). The Ca^{2+} dye was excited with a 543 nm Helium Neon Laser system (Melles Griot 05-LGR-193-381) coupled to a Nikon C2-confocal FN1- upright microscope and emission fluorescence at 552-617 nm was recorded at 18 images/s. Using the Nikon imaging system NIS-Elements, numerous hot spots at the base of the IHCs were identified and recorded during voltage-stimulation. Fluorescence emission was subsequently measured with ImageJ software by drawing a region of interest of 1 μm^2 at the synaptic zones below the nucleus (Fig.9B). Emission fluorescent signals were analyzed and normalized by the ratio F/F_{min} ratio, where F_{min} was the minimum fluorescence found before starting stimulation.

Statistical analysis

Results were analyzed with OriginPro 9.1software (OriginLab, Northampton, USA). Results were analyzed with OriginPro 9.1software (OriginLab, Northampton, USA). Data were tested for normal distribution using the Shapiro-Wilk normality test, and parametric or nonparametric tests were applied accordingly. For statistical analyses with two data sets, two-

tailed unpaired t-tests or two-sided Mann-Whitney tests were used. For comparisons of more than two data sets, one-way ANOVA or two-way ANOVA followed by Tukey multiple comparison test were used when data was normally distributed. If a data set was not normally distributed Kruskal-Wallis tests followed by Dunn multiple comparison tests, respectively, was used. When more than two data sets were compared and significant differences were found, reported p values correspond to the post-hoc multiple comparison test. Values of $p < 0.05$ were considered significant. Results are expressed as mean ± SEM.

RESULTS

Hearing loss

As previously described (Zheng et al., 1999; Zhou et al., 2006), CBA/J mice, used here as a reference, showed no sign of rapid degradation of their hearing function with aging, as attested by constant click ABR thresholds near 15 dB SPL up to one year of age (Fig.1A). On the contrary, C57BL/6J mice, carrying the *Cdh23*^{753A} mutation, displayed an early progressive increase in ABR thresholds with aging (Fig.1A). Hearing thresholds started to increase significantly at postnatal day P180 to reach a mean 50 dB increase at P360 as compared to young mature P30 mice. Distortion product otoacoustic emissions (DPOAEs) in P360 C57BL/6J mice were still present but significantly reduced, indicating that the electromechanical activity of the outer hair cells (OHCs) was also affected (Fig.1B). However, counting hair cells on surface preparations of organs of Corti from these P360 mice, in the mid-cochlea region (8-16 kHz), indicated only a moderate loss of OHCs and IHCs (statistically not significant; Fig.2C), in good agreement with the study of Zachary and Fuchs (2015). This moderate loss of OHCs suggested that the profound hearing loss occurring at P360 in C57BL/6J mice arose from additional factors than a simple alteration of the cochlear amplifier. ABR wave-I amplitude, resulting from the synchronous activity of the auditory nerve fibers, can provide an objective measure of ribbon synapses loss when measured at high sound intensity above 70 dB SPL. In P360 old mice, ABR wave-I amplitudes were largely reduced as compared to young mature P30 mice, even at high sound intensity where IHCs are directly stimulated, bypassing the amplification process of the OHCs (Fig.1C). The decrease in wave-I amplitude indicated a decreased number of auditory nerve fibers activated by sound and/or a decrease in their firing rate or synchrony. The latency of the ABR wave-I was not significantly affected (Fig.1D).

Loss of IHC synaptic ribbons

Immunohistochemical analysis of the synaptic ribbons in IHCs from C57BL/6J mice, in the cochlear region encoding between 8-16 kHz, showed a progressive and large decrease in the number of synaptic ribbons with aging, from 16.3 ± 0.3 ribbons/IHC at P15 to 8.7 ± 0.5 ribbons/IHC at P365 (Fig. 2A-B). This nearly 50% loss of synaptic ribbons in IHCs of C57BL/6J mice at P360 is in good agreement with the study of Zachary and Fuchs (2015).

As previously described (Roux et al., 2006), *Otof*$^{-/-}$ C57BL/6J mice lacking otoferlin are profoundly deaf, with no detectable ABR waves at 90 dB SPL and at all ages tested from P15 to P360 (Fig.1A). The lack of ABR waves arises from a severe defect of Ca^{2+}-evoked synaptic vesicle exocytosis at IHC ribbon synapses (Michalski et al., 2017). This hair cell synaptopathy is associated with an early loss of ribbons at P16 (Vincent et al, 2017; Tertrais et al., 2019). We confirmed here that *Otof*$^{-/-}$ mice have IHCs with an early low number of synaptic ribbons, with a 34% reduction in ribbon number at P15 as compared to P15 *Otof*$^{+/+}$ C57BL/6J mice (10.7 ± 0.3 and 16.3 ± 0.3 synaptic ribbon/IHC, respectively, $p < 0.05$; Fig. 2A-B). The question addressed here was to determine whether this early low number of synaptic ribbons per IHCs further decreased with aging in *Otof*$^{-/-}$ C57BL/6J mice. We found that *Otof*$^{-/-}$ IHCs lose additional synaptic ribbons with aging to reach a very low value of 6.6 ± 0.5 ribbon/IHC at P365 as measured in the cochlear region encoding between 8-16 kHz (Fig.2B), a value significantly lower as compared to *Otof*$^{+/+}$ C57BL/6J mice at comparable age ($p < 0.05$, two-way ANOVA). The loss of presynaptic ribbons, in both *Otof* $^{+/+}$ C57BL/6J (not shown) and *Otof* $^{-/-}$ C57BL/6J mice, was associated with a comparable loss of postsynaptic boutons contacting the IHCs, the afferent nerve terminals being labeled with the dye tracing dextran amine 3000 (Fig. 3). Counting the spiral ganglion neurons in the mid-frequency region of the cochlea (8-16 kHz) showed a similar loss of neurons in P30 *Otof* $^{-/-}$ C57BL/6J mice and P360 *Otof* $^{+/+}$ C57BL/6J mice (Fig. 4). Remarkably, the age-related loss of neurons, averaging 20 %, was much less pronounced than the loss of IHC synaptic ribbons (50 %), suggesting that there is a large number of neurons surviving without dendritic/synaptic projection toward the organ of Corti.

Overall, these results indicated that the deletion of otoferlin exacerbated the loss in synaptic ribbon synapses in IHCs from C57BL/6J mice with aging and indicated that this age-related degenerative process was independent of synaptic vesicle exocytosis and glutamate excitotoxicity.

IHCs become smaller with remaining synaptic ribbons being larger

When analyzing the 3-D imaging reconstruction of the IHC synaptic ribbons from aging C57BL/6J IHCs from high resolution confocal STED immunofluorescent sections, we found that these structures displayed a progressive increase in their mean size (volume) (Fig.5A). The mean volume of the synaptic ribbons increased nearly three-fold between P15 and P365, from ~0.2 μm^3 to 0.6 μm^3 (Fig.5B). Interestingly, the increase in size of the ribbons started

very early at P30, an age at which their number also started to decrease (Fig.2B) while hearing thresholds were normal (Fig.1A).

A similar increase in ribbon size was found in IHCs of C57BL/6J *Otof*$^{-/-}$ mice with aging (Fig.5B). However, the topographical distribution of the ribbons within the infra-nuclear synaptic zone of the *Otof* $^{-/-}$ IHCs was different as compared to *Otof* $^{+/+}$ C57BL/6J mice. The synaptic ribbons of *Otof* $^{-/-}$ IHCs aggregated at the basal infra-nuclear pole of the IHCs (Fig.2A, Fig.6B). The mean inter-distance between each synaptic ribbons was found significantly reduced in *Otof*$^{-/-}$ mice as compared to *Otof* $^{+/+}$ C57BL/6J mice (Fig.5C). The mean inter-distance between ribbons remained rather constant with aging in both mouse strains.

Why the synaptic ribbons are more compactly organized at the basal pole of *Otof* $^{-/-}$ IHCs? To investigate whether this collapse in the inter-ribbon distance was due to a possible disorganization of the synaptic F-actin in IHCs lacking otoferlin, we treated the organ of Corti with fluorescently-labeled phalloidin, a cyclic peptide toxin that binds to F-actin. As previously described (Vincent et al., 2015), each synaptic ribbon is associated with a synaptic F-actin ring, a structure that organizes and delineates the topography of the ribbon active zone at the synaptic basal pole of the IHCs (Fig.6). In the present study, despite the loss of ribbons and their increase in size, the organization of the synaptic F-actin ring network was observed to be similar in IHCs of *Otof* $^{+/+}$ C57BL/6J mice at all the different age studied from P15 to P365 (Fig.6A,A1). However, we found that the F-actin ring organization around the synaptic ribbons was absent as early as P15 in IHCs lacking otoferlin and this structural disorganization may explain the aggregation of the remaining synaptic ribbons at the bottom of the IHCs (Fig. 6B,B1).

When labeling the IHCs cytosol with an antibody against myo-7a, an unconventional myosin essential for the hair bundle functional integrity and found in the apical sterocilia as well as the cytoplasm of the hair cells (Hasson et al., 1995), we measured a drastic reduction in length of the infra-nuclear synaptic zone of *Otof*$^{-/-}$ IHCs lacking otoferlin (Fig.7). The reduction of the IHC synaptic zone was consistent with a large reduction of the resting cell membrane capacitance, measured under whole-cell patch clamp at -70 mV, in P21 *Otof* $^{-/-}$ IHCs as compared to P21*Otof* $^{+/+}$ IHCs (respectively, 8.7 ± 0.1 fF, n = 23, and 10.8 ± 0.1 fF, n = 44, $p < 0.05$), as previously described (Tertrais et al., 2019). Similar reduction in the infra-nuclear IHC synaptic zone, as well as a reduced resting membrane capacitance, was observed in old P360 *Otof* $^{+/+}$ IHCs (Fig. 7). These results indicated that the degenerative process of the

ribbon synapses was associated with a concomitant reduction of the cell surface membrane of IHCs during aging, suggesting a largely augmented uptake of plasma membrane through endocytosis. This process was otoferlin-independent since it was observed in *Otof* $^{-/-}$ IHCs.

Aging promotes autophagy in IHCs through the recruitment of LC3B

Like other type of cells, such as neurons or retinal cells, auditory hair cells utilize autophagic pathways to maintain cell homeostasis during excessive ROS production (Defourny et al., 2019; Fu et al., 2018). Autophagy is a degradation process where cytoplasmic and plasma membrane components are engulfed by vesicles called autophagosomes. To determine whether this process could explain the IHC size reduction with aging, we investigated the recruitment of LC3B, a structural protein of autophagosomal membranes. We assessed and compared the autophagosome numbers and surface area in young P30 and old P365 IHCs by quantifying LC3B puncta numbers/cell by using confocal immunofluoresence. We found that the number and overall surface area of LC3-positive structures in IHCs largely increased with aging (Fig. 8), indicating an increased autophagosome formation. Similar investigations in P365 CBA/J mice, a strain which does not display early age-related hearing loss (Fig. 1), showed weaker expression of LC3B in IHCs (Fig.8).

Higher Ca^{2+} current density and exocytosis in old IHCs

Although the loss IHC ribbon synapses in C57BL/6J mice with aging is well documented in the literature (see Wan and Corfas, 2015), the functional changes of the remaining "old" IHC ribbon synapses has not been yet explored. We investigated here the changes in the calcium-evoked exocytotic responses of aging IHCs from ex-vivo explants of the organ of Corti from aging C57BL/6J mice. We recall that Ca^{2+} is a key messenger for normal hearing since it tunes the transduction of the analogic sound signal into nerve impulses. This transduction occurs at the IHC synaptic active zone through the voltage-activation of $Ca_v1.3$ Ca^{2+} channels (Brandt et al., 2003; Vincent et al., 2017) and the action of the Ca^{2+} sensor otoferlin (Roux et al., 2006; Michalski et al., 2017). Increase in the density of L-type Ca^{2+} channels has long been recognized as a characteristic of aging central neurons (Thibault and Landfield, 1996; Campbell et al., 1996) but possible altered function in Ca^{2+} signaling has never investigated in aging IHCs.

In the present study, whole cell patch-clamp recordings from old P365 IHCs showed a signidicantly increase in Ca^{2+} current density as compared to young mature P30 IHCs, rising

from a mean value of 15.8 pA/pF to 20.1 pA/pF at -10 mV (Fig.9A). The voltage-activation curve of the Ca^{2+} currents in old P365 IHCs remained similar to the young mature P30 IHCs, with a mean half-voltage activation at -29.3 and -26.7 mV, respectively. Intracellular Ca^{2+} imaging during short 100 ms voltage-steps (from -80 mV to -10 mV) indicated higher Ca^{2+} hot spots at the basal synaptic area of old P365 IHCs as compared to young P30 IHCs, suggesting that the density of Ca^{2+} channels at the ribbon active zones of old P365 IHCs was larger (Fig. 9B-C). As a consequence, measurements of membrane capacitance changes indicated larger exocytosis per ribbon active zones in old P365 IHCs (Fig. 9D).

Large decrease in BK channels expression with aging in IHCs

There is increasing evidence that oxydative damage due to an increase in ROS levels plays a crucial role in age-related degeneration of the synaptic ribbon synapses (Fu et al., 2018; Rousset et al., 2020). BK ($K_{Ca1.1}$) channels are known to be highly sensitive to oxydative stress and their activity is a good indicator of intracellular ROS production (Sahoo et al., 2014; Hermann et al., 2015). Interestingly, a decrease in BK channel expression in IHCs has been associated to noise-related ROS and peroxysome pathology (Delmaghani et al., 2015) but never yet described in IHCs during age-relate hearing loss. It is worth recalling that BK channels allows fast repolarization of IHCs and are essential for phase-locking of the auditory afferent neurons (Kros et al., 1998; Skinner et al., 2003; Oliver et al., 2006; Kurt et al., 2012). We here investigated, using immunofluorescent confocal microscopy, the comparative level expression of BK channels in IHCs from young (P30) and old P365 C57BL/6J mice. In young mature IHCs, BK channels are known to be organized in a dozen of clusters at the neck of the IHCs below the cuticular plate (Pyott et al., 2004; Hafidi et al., 2005). We used three-dimensional reconstructions from stacks of confocal images of immunostained organs of Corti (mid- cochlear frequency region 8-16 kHz) to determine the mean total surface area of the BK clusters per IHCs (Fig.10). The results indicated that the expression of BK channels was reduced almost threefold in P360 IHCs as compared to P30 IHCs. A similar threefold reduction in BK channel expression was observed in IHCs from young P30 *Otof* $^{-/-}$ C57BL/6J mice lacking otoferlin. With aging, IHCs from P365 *Otof* $^{-/-}$ C57BL/6J mice showed a further decrease in BK channel expression, reaching nearly one tenth of those observed in P30 *Otof* $^{+/+}$ C57BL/6J. Taken together, these results showed that age-related hearing loss in C57BL/6J mice is associated with a large decreased in BK channel expression in IHCs and that the lack of otoferlin seemed to accelerate this phenomenon.

DISCUSSION

Larger synaptic ribbons associated with larger Ca^{2+} signals

Ribbons are presynaptic organelles tethering glutamate-filled vesicles at the hair cell active zone (AZ). These intracellular structures, composed of the protein RIBEYE, are anchored by the scaffold protein bassoon to the AZ plasma membrane, adjacent to Ca^{2+} $Ca_V1.3$ channels (Brandt et al, 2003; Graydon et al., 2011; Jing et al., 2013; Vincent et al., 2017). Ribbons are essential for high rate of transmitter release and for high temporal precision of neuronal encoding of sound at the auditory afferent nerve fibers (Jean et al., 2018). Each auditory IHC have 10 to 20 synaptic ribbons depending of their cochlear frequency location (Meyer et al., 2009). Ribbons are heterogeneous in size and each ribbon makes a single synaptic contact with one afferent nerve fiber. Remarkably, synapses with larger ribbons have a low rate of spontaneous release and correspond to high-threshold auditory nerve fibers, while synapses with smaller ribbons have a higher rate of spontaneous release and correspond to low-threshold nerve fibers (Liberman et al., 2011). How each type of presynaptic ribbon specifies the activity of each type of afferent nerve fiber still remains unknown. In our study, one of the most striking observations was that IHC synaptic ribbons underwent a nearly threefold increase in size with aging, confirming a certain degree of plasticity of these synaptic structures. The enlargement of the presynaptic ribbons in aging C57BL/6J mice was in good agreement with a previous ultrastructural study by Stamataki et al. (2006). Interestingly, the size of the IHC synaptic ribbons is known to correlate positively with the AZ Ca^{2+} microdomain amplitude, as well as the number and gating of the $Ca_v1.3$ Ca^{2+} channels (Frank et al., 2009; Neef et al., 2018). Also, hair cells of transgenic zebrafish with enlarged ribbons display larger ribbon-localized Ca^{2+} currents (Sheets et al., 2017). In agreement with these previous studies, we found here in aging IHCs that the remaining larger ribbons were associated with larger Ca^{2+} microdomain amplitude, and larger density of calcium currents, that were able to trigger larger exocytotic responses. Overall, these results suggested that the remaining aging ribbon synapses are structurally related to synapses with high-threshold and low-spontaneous activity, likely explaining in part the rise in ABR wave-I thresholds and decreased amplitude in aging C57BL/6J mice. Our description of larger Ca^{2+}-evoked synaptic responses in IHCs of aged C57BL/6J mice could explain the hyperacusis-like exaggeration of the acoustic startle reflex described in these mice (Ison et al., 2007).

One of the most intriguing question is to elucidate the molecular mechanisms determining the intrinsic size of the synaptic ribbons. It is worth recalling that the main structural protein component of ribbons, RIBEYE, is composed of two functional domains: a specific A domain mediating assembly of RIBEYE into large structures and a B domain, identical to CtBP2, binding NAD^+ with high affinity similar to 2-hydroxyacid dehydrogenases (Schmitz et al., 2000). Interestingly, direct application of NAD^+ or NADH to mature zebrafish hair cells increases or decreases ribbon size respectively, possibly acting through the NAD^+ binding site of the B domain of RIBEYE (Wong et al., 2019). In vitro work has shown that NAD^+ and NADH can promote interactions between ribeye domains (Magupalli et al., 2008) and the size of the ribbons would be then sensitive to the subcellular synaptic NAD^+/NADH redox level (Wong et al., 2019). Recent findings suggest the NADH oxidase 3 (NOX3) and its subunit $p22^{phox}$, forming an enzymatic complex generating ROS and highly express in the inner ear, are key factors in generating ARHL and ribbon synapse degeneration in A/J mice (Rousset et al., 2015; 2020). Overall these results suggested that the increase in size of the ribbons in IHCs from aged C57BL/6J mice is a good indicator of NAD^+/NADH homeostasis disruption.

Remarkably, IHCs from C57BL/6J mice lacking otoferlin showed an early, accelerated, loss of synaptic ribbons with aging. In *Otof*$^{-/-}$ IHCs, the remaining ribbons had also a tendency to become larger with age. In mice lacking the vesicular glutamate transporter-3 (Vglut3 KO), IHC ribbons also become larger (Kim et al., 2019). These results indicated that the ribbon enlargement process was independent of synaptic glutamatergic transmission since it was also observed in silent synapses, either lacking otoferlin or Vglut3. The enlargement of the ribbons likely reflected an accelerated intracellular NAD^+/NADH imbalance in these silent synapses. Another remarkable feature observed in *Otof*$^{-/-}$ ribbons was their more compact organization at the IHC infra-nuclear synaptic basal membrane where the network of synaptic F-actin was severely disorganized. We propose that otoferlin, in addition to its key role as calcium sensor for exocytosis (Beurg et al., 2010; Michalski et al., 2017), is also essential for the maintenance of the submembranous synaptic F-actin network. Note that the disruption of this synaptic F-actin network by the marine sponge toxin, latrunculin, was previously shown to rapidly disorganize the spatial distribution of the ribbons and the $Ca_V1.3$ calcium channels (Vincent et al., 2015). Also, the lack of clarin-1, a tetraspan-like membrane protein defective in Usher syndrome type IIIA, was shown to disorganize the synaptic F-actin network and the $Ca_V1.3$ Ca^{2+} channels at the IHCs AZ (Dulon et al., 2018).

IHC shrinkage and loss of BK channels

Another novel observation of our study was the drastic reduction in cell size of IHCs from aging C57BL/6J mice. Interestingly, tuberous sclerosis rapamycin-sensitive complex 1 (mTORC1) has been shown to be overactivated and promote oxidative damages to synapse ribbon loss in aging C57BL/6 mice (Fu et al., 2018). We found that aged P365 IHCs had an increase expression of the autophagy marker LC3B. The activation of the mTOR pathway with aging could therefore trigger the cell size reduction of IHCs, by activation of the autophagy pathway, as proposed in many other cell types (Fingar et al., 2002; Fumarola et al., 2005). In addition, our study described another novel remarkable feature of aging IHCs, a drastic loss of BK channels, suggesting that these potassium channels are also a good indicator of the NAD^+/NADH redox state and autophagy in IHCs. The expression and distribution of BK channels can be regulated through the rapamycin insensitive mTOR complex 2 (mTORC2) as shown in the kidney glomerulus podocytes (Wang et al., 2019). Interestingly, we found that IHCs from young mature C57BL/6J mice lacking otoferlin, beside the loss of ribbons, also showed an early loss of BK channels, suggesting that these IHCs with silent synapses displayed an early ROS dysfunction. Reduction in BK channel expression was also shown in IHCs from young mature mice lacking the type II transmembrane protease 3 (*TMPRSS3*) prior degeneration (Molina et al., 2013; Tang et al., 2019), suggesting that these IHCs share an early common degenerative process with *Otof*$^{-/-}$ IHCs.

Conclusions

Our study unraveled several novel features of aging in IHCs from C57BL/6J mice (Fig.11): 1) a large reduction in their cell size, 2) a drastic enlargement of their synaptic ribbons, 3) an increased presynaptic Ca^{2+} signaling and 4) a decreased BK channel expression. All these features were also observed in young mature IHCs lacking otoferlin, suggesting that they are common markers indicating abnormal oxidative metabolism leading to ROS imbalance and ribbon synapse degeneration in IHCs.

REFERENCES

Bartolomé MV, del CE, López LM, Carricondo F, Poch-Broto J, Gil-Loyzaga P. Effects of aging on C57BL/6J mice: an electrophysiological and morphological study. Adv Otorhinolaryngol. 2002;59:106-11.

Beurg M, Michalski N, Safieddine S, Bouleau Y, Schneggenburger R, Chapman ER, Petit C, Dulon D. Control of exocytosis by synaptotagmins and otoferlin in auditory hair cells. J Neurosci. 2010 Oct 6;30(40):13281-90.

Brandt A, Striessnig J, Moser T. $Ca_V1.3$ channels are essential for development and presynaptic activity of cochlear inner hair cells [J]. The Journal of neuroscience : the official journal of the Society for Neuroscience, 2003, 23(34): 10832-10840.

Campbell LW, Hao SY, Thibault O, Blalock EM, and. Landfield PW. Aging Changes in Voltage-Gated Calcium Currents in Hippocampal CA1 Neurons. J Neurosci, October 1, 1996, 16(19):6286–6295.

Bolte S, Cordelières FP. A guided tour into subcellular colocalization analysis in light microscopy. J Microsc. 2006 Dec;224(Pt 3):213-32.

Defourny J, Aghaie A, Perfettini I, Avan P, Delmaghani S, Petit C. Pejvakin-mediated pexophagy protects auditory hair cells against noise-induced damage. Proc Natl Acad Sci U S A. 2019 Apr 16;116(16):8010-8017.

Delmaghani S, Defourny J, Aghaie A, Beurg M, Dulon D, Thelen N, Perfettini I, Zelles T, Aller M, Meyer A, Emptoz A, Giraudet F, Leibovici M, Dartevelle S, Soubigou G, Thiry M, Vizi ES, Safieddine S, Hardelin JP, Avan P, Petit C. Hypervulnerability to Sound Exposure through Impaired Adaptive Proliferation of Peroxisomes. Cell. 2015 Nov 5;163(4):894-906. doi: 10.1016/j.cell.2015.10.023

Dulon D, Safieddine S, Jones SM, Petit C. Otoferlin is critical for a highly sensitive and linear calcium-dependent exocytosis at vestibular hair cell ribbon synapses. J Neurosci. 2009 Aug 26;29(34):10474-87.

Dulon D, Papal S, Patni P, Cortese M, Vincent PF, Tertrais M, Emptoz A, Tlili A, Bouleau Y, Michel V, Delmaghani S, Aghaie A, Pepermans E, Alegria-Prevot O, Akil O, Lustig L, Avan P, Safieddine S, Petit C, El-Amraoui A. Clarin-1 gene transfer rescues auditory synaptopathy in model of Usher syndrome. J Clin Invest. 2018 Aug 1;128(8):3382-3401.

Fingar DC, Salama S, Tsou C, Harlow E, Blenis J. Mammalian cell size is controlled by mTOR and its downstream targets S6K1 and 4EBP1/eIF4E. Genes Dev. 2002 Jun 15;16(12):1472-87.

Frank T, Khimich D, Neef A, Moser T. Mechanisms contributing to synaptic Ca2+ signals and their heterogeneity in hair cells. Proc Natl Acad Sci U S A. 2009 Mar 17;106(11):4483-8.

Fritzsch B, Duncan JS, Kersigo J, Gray B, Elliott KL. Neuroanatomical Tracing Techniques in the Ear: History, State of the Art, and Future Developments. Methods Mol Biol. 2016;1427:243-62. doi: 10.1007/978-1-4939-3615-1_14.

Fu X, Sun X, Zhang L, Jin Y, Chai R, Yang L, Zhang A, Liu X, Bai X, Li J, Wang H, Gao J. Tuberous sclerosis complex-mediated mTORC1 overactivation promotes age-related hearing loss. J Clin Invest. 2018 Nov 1;128(11):4938-4955.

Fumarola C, La Monica S, Alfieri RR, Borra E, Guidotti GG. Cell size reduction induced by inhibition of the mTOR/S6K-signaling pathway protects Jurkat cells from apoptosis. Cell Death Differ. 2005 Oct;12(10):1344-57.

Graydon CW, Cho S, Li GL, Kachar B, von Gersdorff H. Sharp Ca^{2+} nanodom ains beneath the ribbon promote highly synchronous multivesicular release at hair cell synapses. J Neurosci. 2011 Nov 16;31(46):16637-50.

Hafidi A, Beurg M, Dulon D. Localization and developmental expression of BK channels in mammalian cochlear hair cells. Neuroscience. 2005;130(2):475-84.

Hasson T, Heintzelman M B, Santos-Sacchi J, Corey D P, and Mooseker M S. Expression in cochlea and retina of myosin VIIa, the gene product defective in Usher syndrome type 1B. PNAS October 10, 1995 92 (21) 9815-9819

Hequembourg S, Liberman MC. Spiral ligament pathology: a major aspect of age-related cochlear degeneration in C57BL/6 mice. J Assoc Res Otolaryngol. 2001 Jun;2(2):118-29.

Henry KR. Sex- and age-related elevation of cochlear nerve envelope response (CNER) and auditory brainstem response (ABR) thresholds in C57BL/6 mice. Hear Res. 2002 Aug;170(1-2):107-15.

Hermann A, Sitdikova GF, Weiger TM. Oxidative Stress and Maxi Calcium-Activated Potassium (BK) Channels. Biomolecules. 2015 Aug 17;5(3):1870-911.

Hu N, Rutherford MA, Green SH. Protection of cochlear synapses from noise-induced excitotoxic trauma by blockade of Ca2+-permeable AMPA receptors. Proc Natl AcadSci U S A. 2020 Feb 18;117(7):3828-3838

Ison JR, Allen PD, O'Neill WE Age-related hearing loss in C57BL/6J mice has both frequency-specific and non-frequency-specific components that produce a hyperacusis-like exaggeration of the acoustic startle reflex. J Assoc Res Otolaryngol. 2007 Dec;8(4):539-50.

Jean P, Lopez de la Morena D, Michanski S, Jaime Tobón LM, Chakrabarti R, Picher MM, Neef J, Jung S, Gültas M, Maxeiner S, Neef A, Wichmann C, Strenzke N, Grabner C, Moser T. The synaptic ribbon is critical for sound encoding at high rates and with temporal precision. eLife 2018;7:e29275.

Jiang XW, Li XR, Zhang YP. Changes of ribbon synapses number of cochlear hair cells in C57BL/6Jmice with age. Int J Clin Exp Med. 2015 Oct 15;8(10):19058-64. eCollection 2015.

Jing Z, Rutherford MA, Takago H, Frank T, Fejtova A, Khimich D, Moser T, Strenzke N. Disruption of the presynaptic cytomatrix protein bassoon degrades ribbon anchorage, multiquantal release, and sound encoding at the hair cell afferent synapse. J Neurosci. 2013 Mar 6;33(10):4456-67. doi: 10.1523/JNEUROSCI.3491-12.2013

Johnson KR, Erway LC, Cook SA, Willott JF, Zheng QY. A major gene affecting age-related hearing loss in C57BL/6J mice. Hear Res. 1997 Dec;114(1-2):83-92

Kazmierczak P, Sakaguchi H, Tokita J, Wilson-Kubalek EM, Milligan RA, Müller U, Kachar BCadherin 23 and protocadherin 15 interact to form tip-link filaments in sensory hair cells. Nature. 2007 Sep 6;449(7158):87-91.

Kim KX, Payne S, Yang-Hood A, Li SZ, Davis B, Carlquist J, V-Ghaffari B, Gantz JA, Kallogjeri D, Fitzpatrick JAJ, Ohlemiller KK, Hirose K, Rutherford MA. Vesicular Glutamatergic Transmission in Noise-induced Loss and Repair of Cochlear Ribbon Synapses. J Neurosci. 2019 Mar 29. pii: 2228-18. doi: 10.1523/JNEUROSCI.2228-18.2019.

Kros CJ, Ruppersberg JP, Rüsch A. Expression of a potassium current in inner hair cells during development of hearing in mice.Nature. 1998 Jul 16;394(6690):281-4

Kujawa SG, Liberman MC. Synaptopathy in the noise-exposed and aging cochlea: Primary neural degeneration in acquired sensorineural hearing loss. Hear Res. 2015 Dec;330(Pt B):191-9.

Kujawa SG, Liberman MC. Translating animal models to human therapeutics in noise-induced and age-related hearing loss. Hear Res. 2019 Jun; 77:44-52.

Kurt S, Sausbier M, Rüttiger L, Brandt N, Moeller CK, Kindler J, Sausbier U, Zimmermann U, van Straaten H, Neuhuber W, Engel J, Knipper M, Ruth P, Schulze H. Critical role for cochlear hair cell BK channels for coding the temporal structure and dynamic range of auditory information for central auditory processing. FASEB J. 2012 Sep;26(9):3834-43.

Lagziel A, Ahmed ZM, Schultz JM, Morell RJ, Belyantseva IA, Friedman TB. Spatiotemporal pattern and isoforms of cadherin 23 in wild type and waltzer mice during inner ear hair cell development. Dev Biol. 2005 Apr 15;280(2):295-306.

Liberman LD, Wang H, Liberman MC. Opposing gradients of ribbon size and AMPA receptor expression underlie sensitivity differences among cochlear-nerve/hair-cell synapses. J Neurosci. 2011 Jan 19;31(3):801-8.

Magupalli VG, Schwarz K, Alpadi K, Natarajan S, Seigel GM, Schmitz F. 2008. Multiple RIBEYE-RIBEYE interactions create a dynamic scaffold for the formation of synaptic ribbons. Journal of Neuroscience 28:7954– 7967.

Meyer AC, Frank T, Khimich D, Hoch G, Riedel D, Chapochnikov NM, Yarin YM, Harke B, Hell SW, Egner A, Moser T. Tuning of synapse number, structure and function in the cochlea. Nat Neurosci. 2009 Apr;12(4):444-53. doi: 10.1038/nn.2293. Epub 2009 Mar 8.

Michalski N, Goutman JD, Auclair SM, Boutet de Monvel J, Tertrais M, Emptoz A, Parrin A, Nouaille S, Guillon M, Sachse M, Ciric D, Bahloul A, Hardelin JP, Sutton RB, Avan P, Krishnakumar SS, Rothman JE, Dulon D, Safieddine S, Petit C. Otoferlin acts as a Ca^{2+} sensor for vesicle fusion and vesicle pool replenishment at auditory hair cell ribbon synapses. Elife. 2017 Nov 7;6. pii: e31013.

Michel V, Goodyear RJ, Weil D, Marcotti W, Perfettini I, Wolfrum U, Kros CJ, Richardson GP, Petit C. Cadherin 23 is a component of the transient lateral links in the developing hair bundles of cochlear sensory cells. Dev Biol. 2005 Apr 15;280(2):281-94

Mock BE, Vijayakumar S, Pierce J, Jones TA, Jones SM. Differential effects of Cdh23(753A) on auditory and vestibular functional aging in C57BL/6J mice. Neurobiol Aging. 2016 Jul;43:13-22. doi: 10.1016/j.neurobiolaging.2016.03.013. Epub 2016 Mar 26.

Molina L, Fasquelle L, Nouvian R, Salvetat N, Scott HS, Guipponi M, Molina F, Puel JL, Delprat B. Tmprss3 loss of function impairs cochlear inner hair cell Kcnma1 channel membrane expression Hum Mol Genet. 2013 Apr 1;22(7):1289-99. doi: 10.1093/hmg/dds532. Epub 2012 Dec 18.

Neef J, Urban NT, Ohn TL, Frank T, Jean P, Hell SW, Willig KI, Moser T. Quantitative optical nanophysiology of Ca_{2+} signaling at inner hair cell active zones. Nat Commun. 2018 Jan 18;9(1):290. doi: 10.1038/s41467-017-02612-y.

Noben-Trauth K, Zheng QY, Johnson KR. Association of cadherin 23 with polygenic inheritance and genetic modification of sensorineural hearing loss. Nat Genet. 2003 Sep;35(1):21-3. Epub 2003 Aug 10.

Oliver D, Taberner AM, Thurm H, Sausbier M, Arntz C, Ruth P, Fakler B, Liberman MC. The role of BKCa channels in electrical signal encoding in the mammalian auditory periphery.J Neurosci. 2006 Jun 7;26(23):6181-9.

Pujol R, Puel JL. Excitotoxicity, synaptic repair, and functional recovery in the mammalian cochlea: a review of recent findings. Ann N Y Acad Sci. 1999 Nov 28;884:249-54.

Pyott SJ, Glowatzki E, Trimmer JS, Aldrich RW. Extrasynaptic localization of inactivating calcium-activated potassium channels in mouse inner hair cells. J Neurosci. 2004 Oct 27;24(43):9469-74.

Rousset F, Carnesecchi S, Senn P, Krause KH. NOX3-Targeted Therapies for Inner Ear Pathologies.*Curr Pharm Des*. 2015;21(41):5977–5987

Rousset F, Nacher-Soler G, Coelho M, Ilmjarv S, Kokje VBC, Marteyn A, Cambet Y, Perny M, Roccio M, Jaquet V, Senn P, Krause KH. Redox activation of excitatory pathways in auditory neurons as mechanism of age-related hearing loss. Redox Biol. 2020 Feb;30:101434.

Roux I, Safieddine S, Nouvian R, Grati M, Simmler MC, Bahloul A, Perfettini I, Le Gall M, Rostaing P, Hamard G, Triller A, Avan P, Moser T, Petit C. Otoferlin, defective in a human

deafness form, is essential for exocytosis at the auditory ribbon synapse. Cell. 2006 Oct 20;127(2):277-89.

Sahoo N, Hoshi T, Heinemann SH. Oxidative modulation of voltage-gated potassium channels. Antioxid Redox Signal. 2014 Aug 20;21(6):933-52. doi: 10.1089/ars.2013.5614. Epub 2013 Oct 26. Review

Schmitz F, Königstorfer A, Südhof TC. RIBEYE, a component of synaptic ribbons: a protein's journey through evolution provides insight into synaptic ribbon function. Neuron. 2000 Dec;28(3):857-72.

Sheets L, He XJ, Olt J, Schreck M, Petralia RS, Wang YX, Zhang Q, Beirl A, Nicolson T, Marcotti W, Trapani JG, Kindt KS. Enlargement of Ribbons in Zebrafish Hair Cells Increases Calcium Currents But Disrupts Afferent Spontaneous Activity and Timing of Stimulus Onset. J Neurosci. 2017 Jun 28;37(26):6299-6313. doi: 10.1523/JNEUROSCI.2878-16.2017.

Siemens J, Lillo C, Dumont RA, Reynolds A, Williams DS, Gillespie PG, Müller U. Cadherin 23 is a component of the tip link in hair-cell stereocilia. Nature. 2004 Apr 29;428(6986):950-5. Epub 2004 Mar 31.

Skinner LJ, Enée V, Beurg M, Jung HH, Ryan AF, Hafidi A, Aran JM,Dulon D. Contribution of BK Ca2+-activated K+ channels to auditory neurotransmission in the Guinea pig cochlea. J Neurophysiol. 2003 Jul;90(1):320-32.

Söllner C, Rauch GJ, Siemens J, Geisler R, Schuster SC, Müller U, Nicolson T; Tübingen 2000 Screen Consortium. Mutations in cadherin 23 affect tip links in zebrafish sensory hair cells. Nature. 2004 Apr 29;428(6986):955-9.

Spongr VP, Flood DG, Frisina RD, Salvi RJ. Quantitative measures of hair cell loss in CBA and C57BL/6 mice throughout their life spans. J Acoust Soc Am. 1997 Jun;101(6):3546-53.

Stamataki S, Francis HW, Lehar M, May BJ, Ryugo DK. Synaptic alterations at inner hair cells precede spiral ganglion cell loss in aging C57BL/6J mice. Hear Res. 2006 Nov;221(1-2):104-18. Epub 2006 Sep 26

Tang PC, Alex AL, Nie J, Lee J, Roth AA, Booth KT, Koehler KR, Hashino E, Nelson RF. Defective Tmprss3-Associated Hair Cell Degeneration in Inner Ear Organoids. Stem Cell Reports. 2019 Jul 9;13(1):147-162.

Tertrais M, Bouleau Y, Emptoz A, Belleudy S, Sutton RB, Petit C, Safieddine S, Dulon D. Viral transfer of mini-otoferlins partially restores the fast component of exocytosis and uncovers ultrafast endocytosis in auditory hair cells of otoferlin knock-out mice. J Neurosci. 2019 Mar 4. pii: 1550-18. doi: 10.1523/JNEUROSCI.1550-18.2018.

Thibault O and. Landfield PW. Increase in Single L-Type Calcium Channels in Hippocampal Neurons During Aging. Science 1996, 272 : 1017-1020.

Vincent PF, Bouleau Y, Petit C, Dulon D. A synaptic F-actin network controls otoferlin-dependent exocytosis in auditory inner hair cells. Elife. 2015 Nov 14;4.

Vincent PF, Bouleau Y, Safieddine S, Petit C, Dulon D. Exocytotic machineries of vestibular type I and cochlear ribbon synapses display similar intrinsic otoferlin-dependent Ca2+ sensitivity but a different coupling to Ca2+ channels. J Neurosci. 2014 Aug 13;34(33):10853-69.

Vincent PF, Bouleau Y, Charpentier G, Emptoz A, Safieddine S, Petit C, Dulon D. Different $Ca_V1.3$ Channel Isoforms Control Distinct Components of the Synaptic Vesicle Cycle in Auditory Inner Hair Cells. J Neurosci. 2017 Mar 15;37(11):2960-2975.

Wan G, Corfas G. No longer falling on deaf ears: mechanisms of degeneration and regeneration of cochlear ribbon synapses. Hear Res. 2015 Nov;329:1-10.

Wang Y, Tao J, Wang M, Yang L, Ning F, Xin H, Xu X, Cai H, Zhang W, Yu K, Zhang X. Mechanism of Regulation of Big-Conductance Ca^{2+}-Activated K^+ Channels by mTOR Complex 2 in Podocytes. Front Physiol. 2019 Feb 28;10:167. doi: 10.3389/fphys.2019.00167. eCollection 2019.

Wong HC, Zhang Q, Beirl AJ, Petralia RS, Wang YX, Kindt K. Synaptic mitochondria regulate hair-cell synapse size and function. Elife. 2019 Oct 14;8. pii: e48914. doi: 10.7554/eLife.48914.

Zachary SP, Fuchs PA Re-Emergent Inhibition of Cochlear Inner Hair Cells in a Mouse Model of Hearing Loss. J Neurosci. 2015 Jul 1;35(26):9701-6.

Zheng QY, Johnson KR, and Erway LC Assessment of hearing in 80 inbred strains of mice by ABR threshold analyses. Hear Res. 1999, 130(1-2): 94–107.

Zhou, X., Jen, P.H.-S., Seburn, K.L., Frankel, W.N., and Zheng, Q.Y. (2006). Auditory brainstem responses in 10 inbred strains of mice. Brain Research *1091*, 16–26.

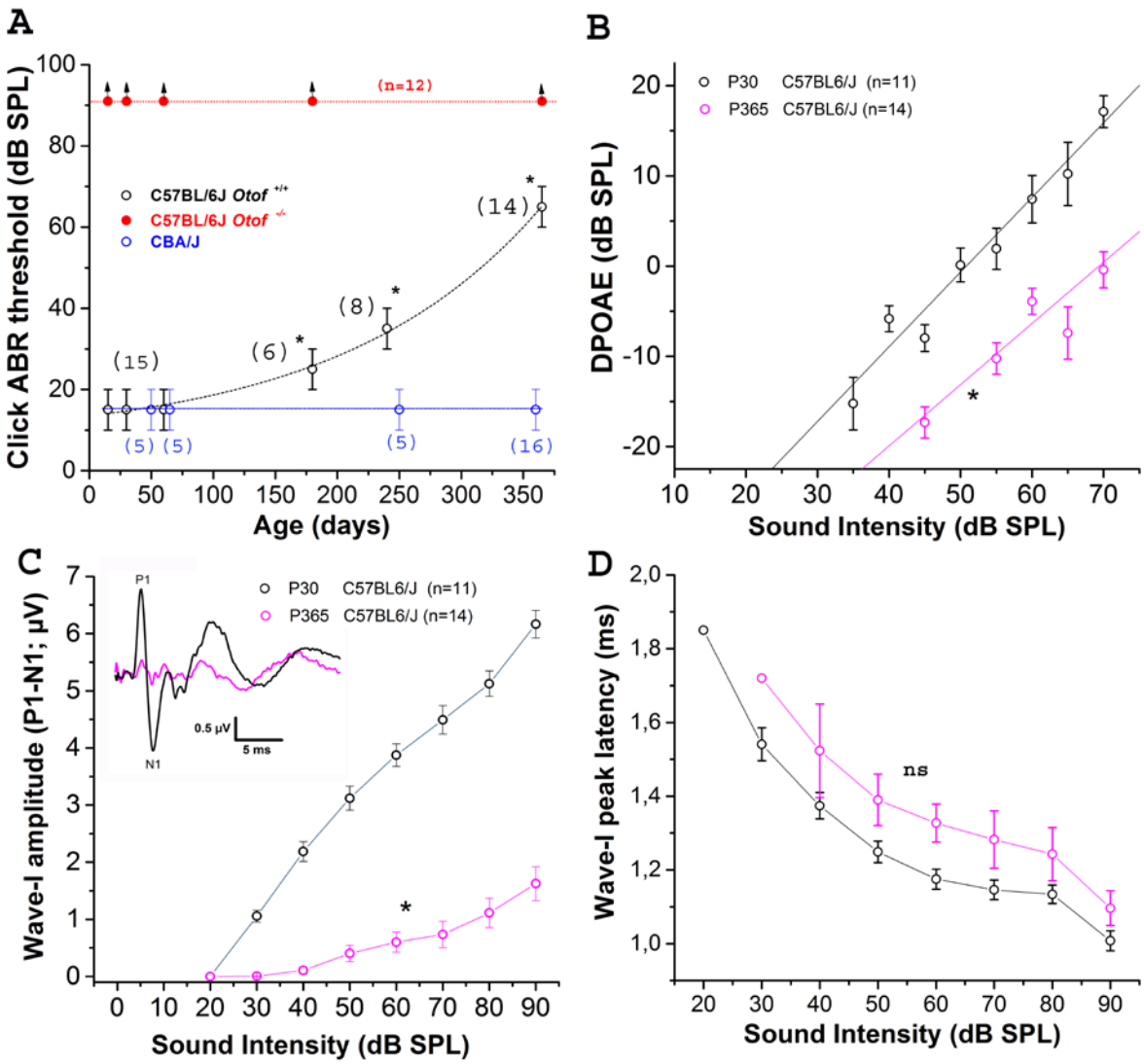

Figure 1: Sensorineural hearing loss with Aging in C57BL/6J mice

A) Click-ABR thresholds as a function of age in CBA/J mice (blue; n = 5 to 16), C57BL/6J *Otof* $^{+/+}$ mice (black; n = 6 to 14) and in C57BL/6J *Otof* $^{-/-}$ mice (red; n = 12). Asterisks indicate significant difference with $p<0.05$ as compared to P30 mice (two-way ANOVA).

B) Distortion products otoacoustic emissions (DPOAEs) as a function of sound intensity in young P30 (black) and old P360 (pink) C57BL/6J *Otof* $^{+/+}$ mice. Asterisks indicate significant difference with $p<0.05$ (two-way ANOVA, $p = 0.01$).

C) Wave-I amplitude as a function of sound intensity in young P30 (black) and old P360 (pink) C57BL/6J *Otof*$^{+/+}$ mice. Inset show comparative mean ABR waves at 70 dB SPL. Asterisks indicate significant difference with $p<0.05$ (two-way ANOVA; $p = 0.001$).

D) Latency to reach peak amplitude of wave-I as a function of sound intensity. Not significantly different (ns) with $p=0.46$ (two-way ANOVA; n is indicated in graph C).

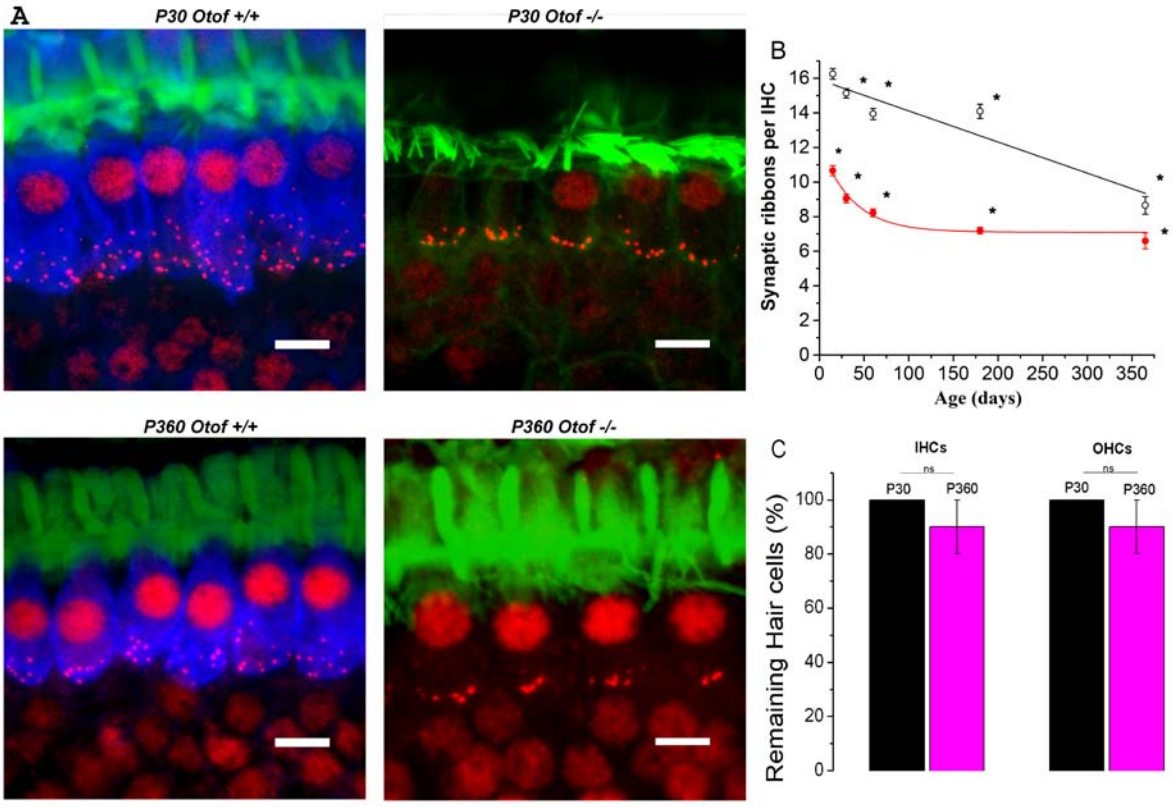

Figure 2: Synaptic ribbon loss in aging IHCs

A) Immuno-confocal imaging of IHCs (stack reconstructions of ten 1µm slices) showing F-actin (green, labeling the hair bundles), otoferlin (blue; a synaptic Ca^{2+} sensor labeling the entire IHC body, absent in *Otof* $^{-/-}$) and the synaptic ribbons (Ribeye/CtBP2, red dots). The white bars indicate 8 µm.

B) Plot of synaptic ribbon counts per IHC as a function of age in C57BL/6J *Otof*$^{+/+}$ mice (black) and in C57BL/6J *Otof* $^{-/-}$ mice in the mid-frequency cochlear region (8-16 kHz). Asterisks indicate significant difference with $p<0.05$ (comparison with P15 C57BL/6J *Otof*$^{+/+}$ mice, two-way ANOVA post-hoc Tukey test). For C57BL/6J *Otof* $^{+/+}$ mice (3 to 5 mice at each age), 203, 306, 306, 306, 295 ribbons were respectively analyzed at P15, P30, P60, P180, P365. For C57BL/6J *Otof* $^{-/-}$ mice (3 mice at each age), 194, 294, 264, 167 and 100 ribbons were analyzed respectively at P15, P30, P60, P180, P365.

C) Comparative hair cell counts in the mid-frequency cochlear region (8-16 kHz) of young P30 (black; n=3 mice) and old P365 (pink, n=3 mice) C57BL/6J *Otof*$^{+/+}$ mice. Statistical analysis indicated no significant difference with $p = 0.37$ (n = 50 IHCs at P30 and P360) and $p = 0.14$ (n =170 OHCs at P30 and P360) using unpaired-t test.

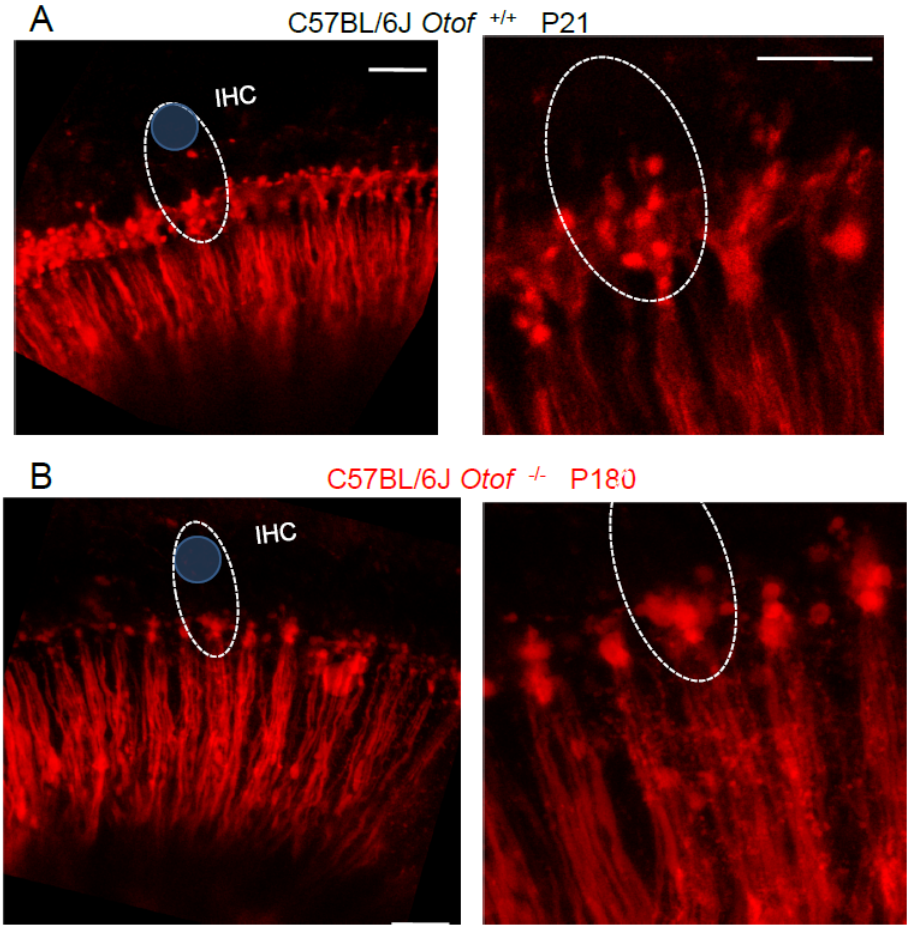

Figure 3: Comparative dye labeling (dextran amines 3000) of afferent nerve fibers and synaptic bouton below IHCs in young mature C57BL/6J *Otof*$^{+/+}$ mice and P180 C57BL/6J *Otof* $^{-/-}$ mice.

Note a significant loss of afferent nerve fibers and synaptic boutons in IHCs (position indicated by the dotted line) lacking otoferlin. A similar loss of afferent fibers was observed in old P365 *Otof* $^{+/+}$ mice (not shown).White apical bars indicate 10 µm.

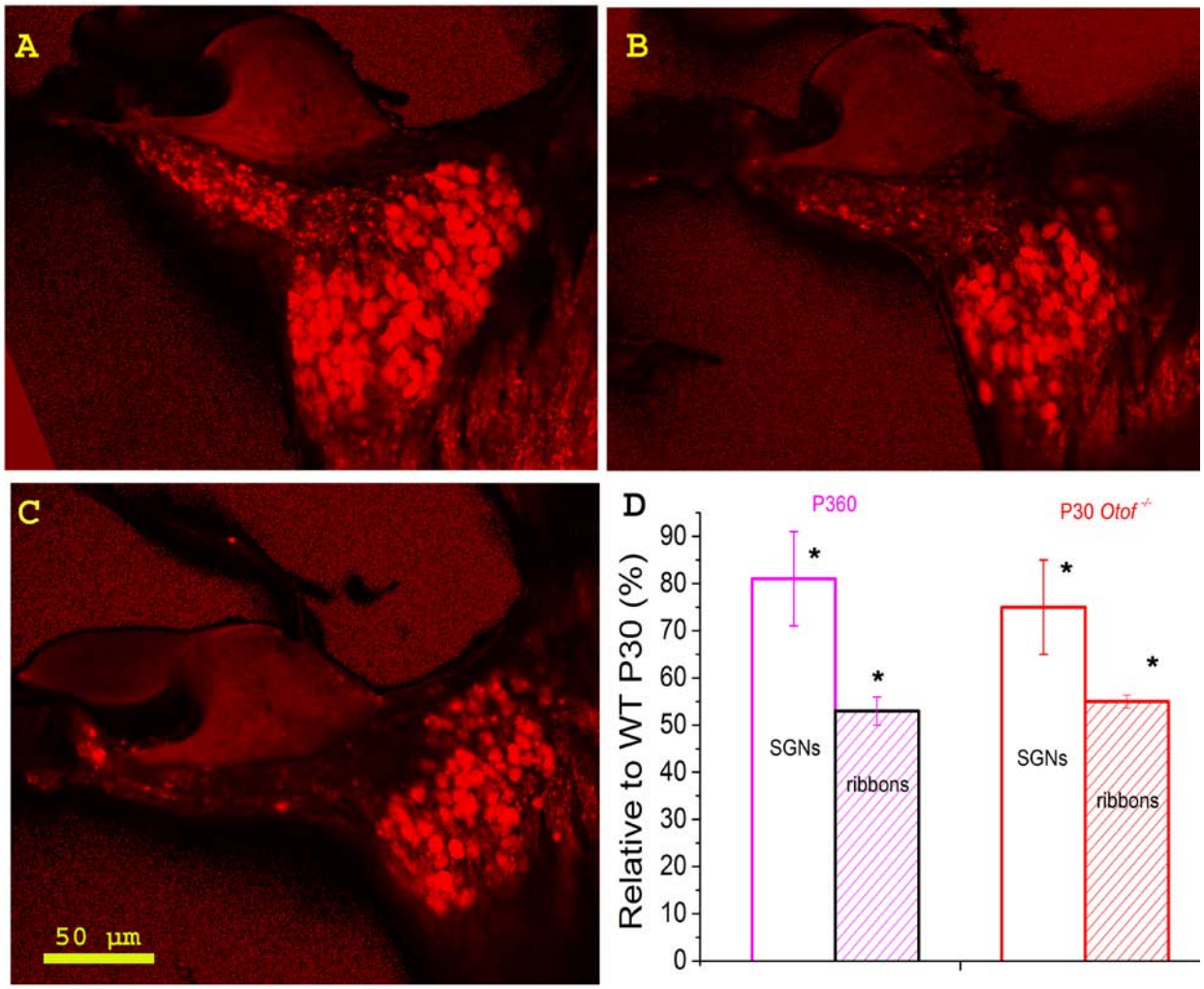

Figure 4: Comparative density of spiral ganglion neurons (SGNs) labeled with the fluorescent dye dextran 3000

A) In a cochlea of young mature P30 of C57BL/6J *Otof* $^{+/+}$ mouse
B) In P30 C57BL/6J *Otof* $^{-/-}$ mice
C) In old P365 C57BL/6J *Otof* $^{+/+}$ mice. Note the reduction in SGNs and the drastic decrease of the fluorescent labeling of the afferent nerve fibers projecting to the organ of Corti.
D) Analyzed in the mid-cochlea (8-16kHz), comparative histogram of remaining SGNs (n=3 cochleae) and synaptic ribbons (P360 *Otof*$^{+/+}$ n = 295; P30 *Otof* $^{-/-}$ n = 194) relative to young mature P30 C57BL/6J *Otof* $^{+/+}$ mice (n= 3 cochlea and n = 203 ribbons). The asterisks indicated statistical difference with $p < 0.05$ (from left to right p = 0.020 and p = 0.018 for SGNs and p = 1.01E-14 and p = 1.69E-14 for ribbons, one-way ANOVA post-hoc Tukey test).

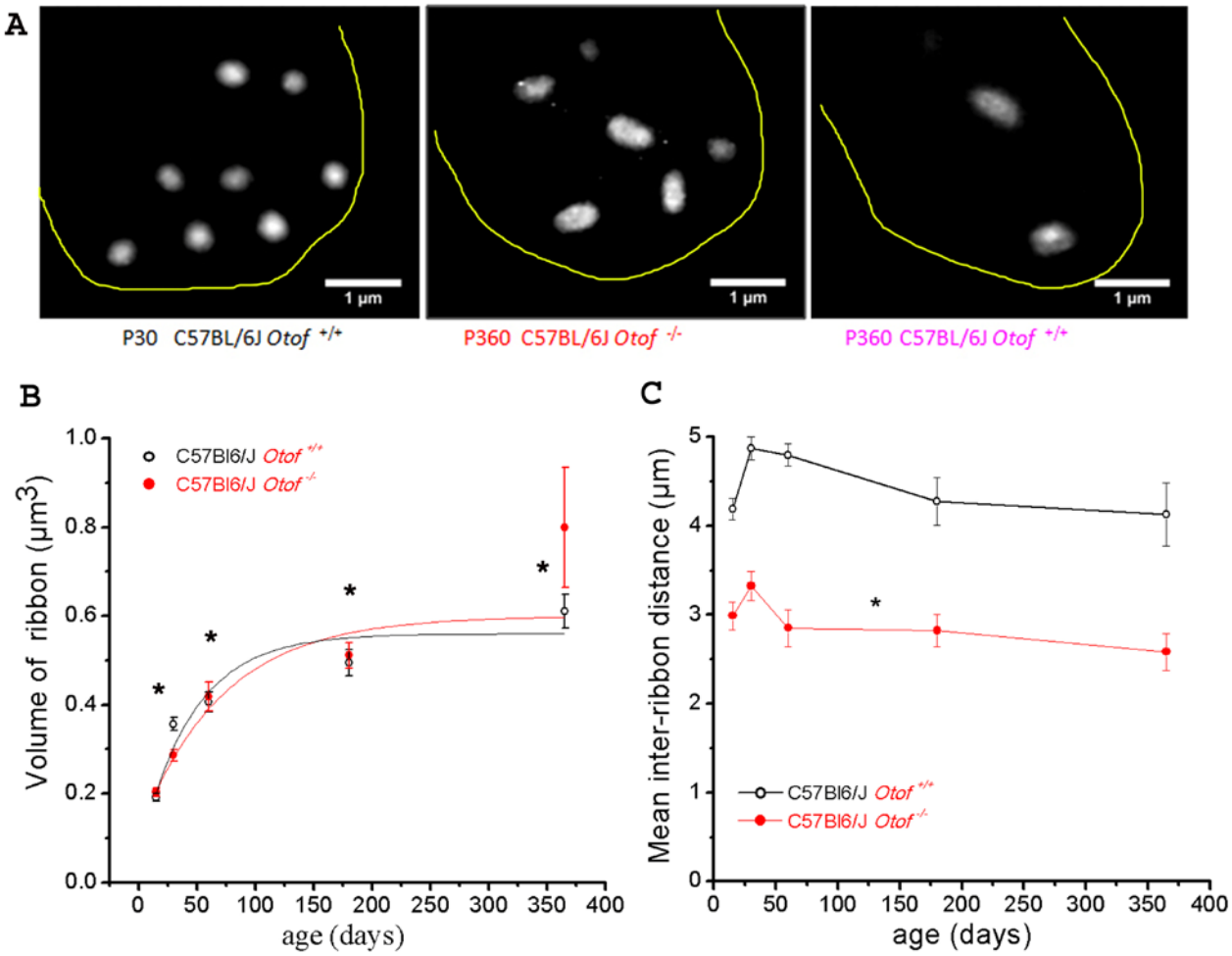

Figure 5: Size and inter-distance between synaptic ribbons with aging

A) Example of high magnification confocal STED images (stack reconstruction of five 0.25 µm slices). The yellow line delineates the IHC contour. Note larger single ribbons in old P360 IHCs.

B) The volume of the synaptic ribbons increased in a similar manner with aging in C57BL/6J *Otof* $^{+/+}$ (black) and C57BL/6J *Otof* $^{-/-}$ (red). As indicated by the asterisks, when comparing with P15 for each strain, the volume of the ribbon started significantly to increase significantly from P30 ($p<0.05$; two-way ANOVA).

C) Mean inter-ribbon distances with aging in IHCs from C57BL/6J *Otof* $^{+/+}$ (black) and C57BL/6J *Otof* $^{-/-}$ (red). Note that the mean inter-ribbon distance is smaller in *Otof* $^{-/-}$ IHCs, where they aggregate at the basal pole of the cells (see Fig. 2A), as compared to *Otof* $^{+/+}$ IHCs (* for $p < 0.05$; two-way ANOVA). The number of ribbons analyzed at each age is indicated in the legend of Fig. 2.

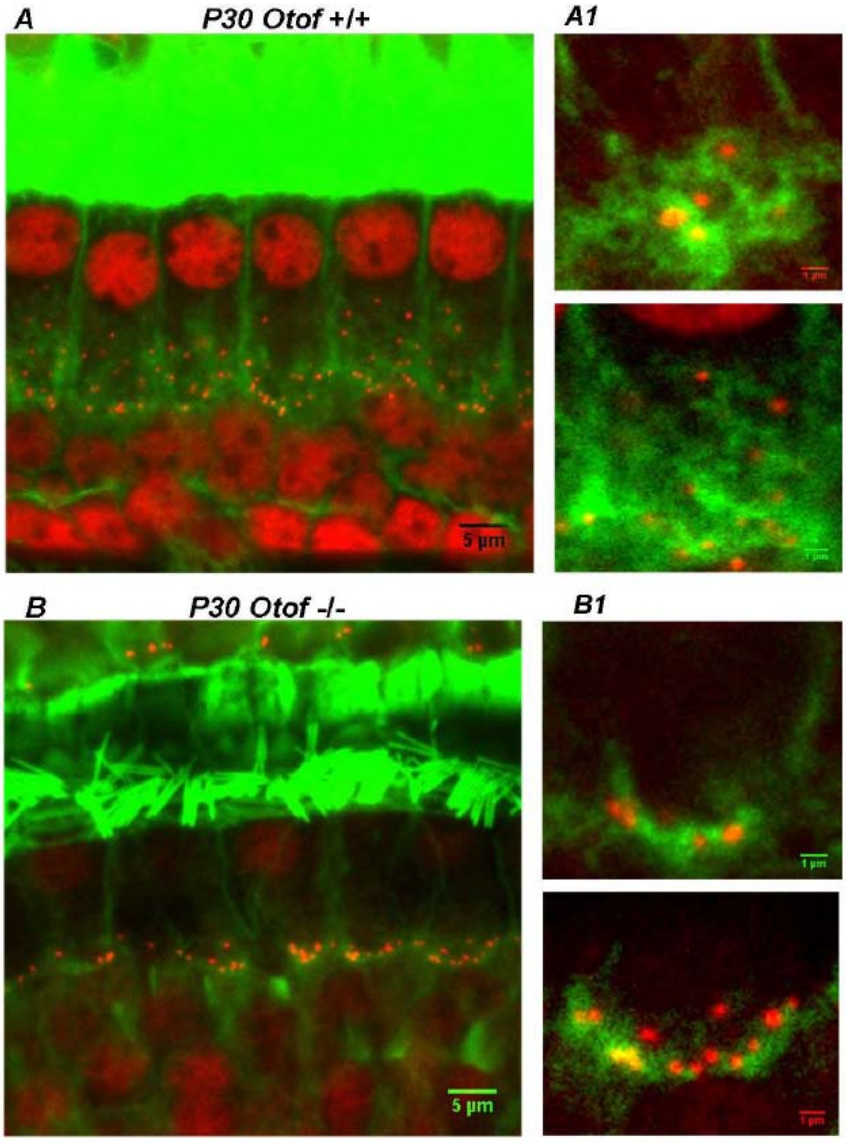

Figure 6: Comparative organization of F-actin at the IHC ribbon synapses of C57BL/6J *Otof* $^{+/+}$ mice (A, A1) and C57BL/6J *Otof* $^{-/-}$ mice (B, B1).

While F-actin delineated structural cages around individual ribbons in *Otof* $^{+/+}$ IHCs (A1, top image corresponded to P30 and bottom image to P365), this organization was absent in *Otof* $^{-/-}$ IHCs where ribbons aggregated at the basal membrane of the cells (B1 top image=P180 and bottom = P30).

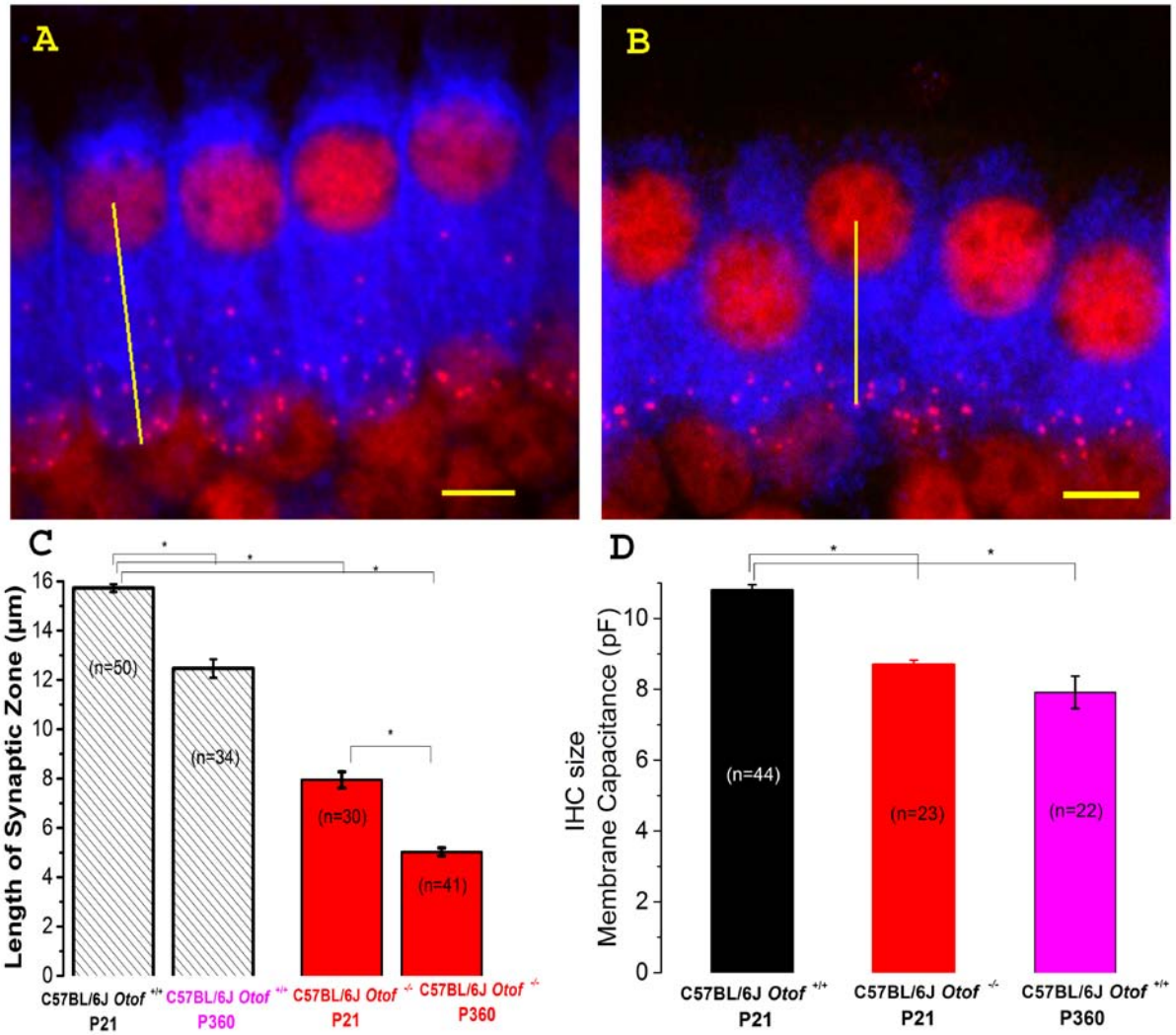

Figure 7: Size reduction of the basal infra-nuclear synaptic zone of IHCs with aging in presence or absence of otoferlin

Immunoconfocal imaging of IHCs from P21 C57BL/6J *Otof* $^{+/+}$ (A) and P21C57BL/6J *Otof* $^{-/-}$ (B). IHCs were labeled for myo-7a (blue) and CtBP2 (labeling the ribbons, red). The size of the infra-nuclear synaptic zone was measured from the middle of the nucleus to the bottom of the cell as indicated with the yellow line. The scale bar indicated 5 µm.

C) Comparative histogram of the length of the infra-nuclear synaptic zone with aging in presence (grey) or absence of otoferlin (red). Asterisks indicated statistical significance with $p<0.05$ (comparison from left to right with p= 1.18E-14; 2.5E-36; 7.83E-63; 3,09E-12; one-way ANOVA post-hoc Tukey test).

D) Comparative IHC resting membrane capacitance measured at -70 mV in patch-clamp whole cell recording. Asterisks indicated values with significant difference with $p < 0.05$ (comparison from right to lelft: p = 6.16E-8, p = 2.8E-12; one-way ANOVA post-hoc Bonferroni test).

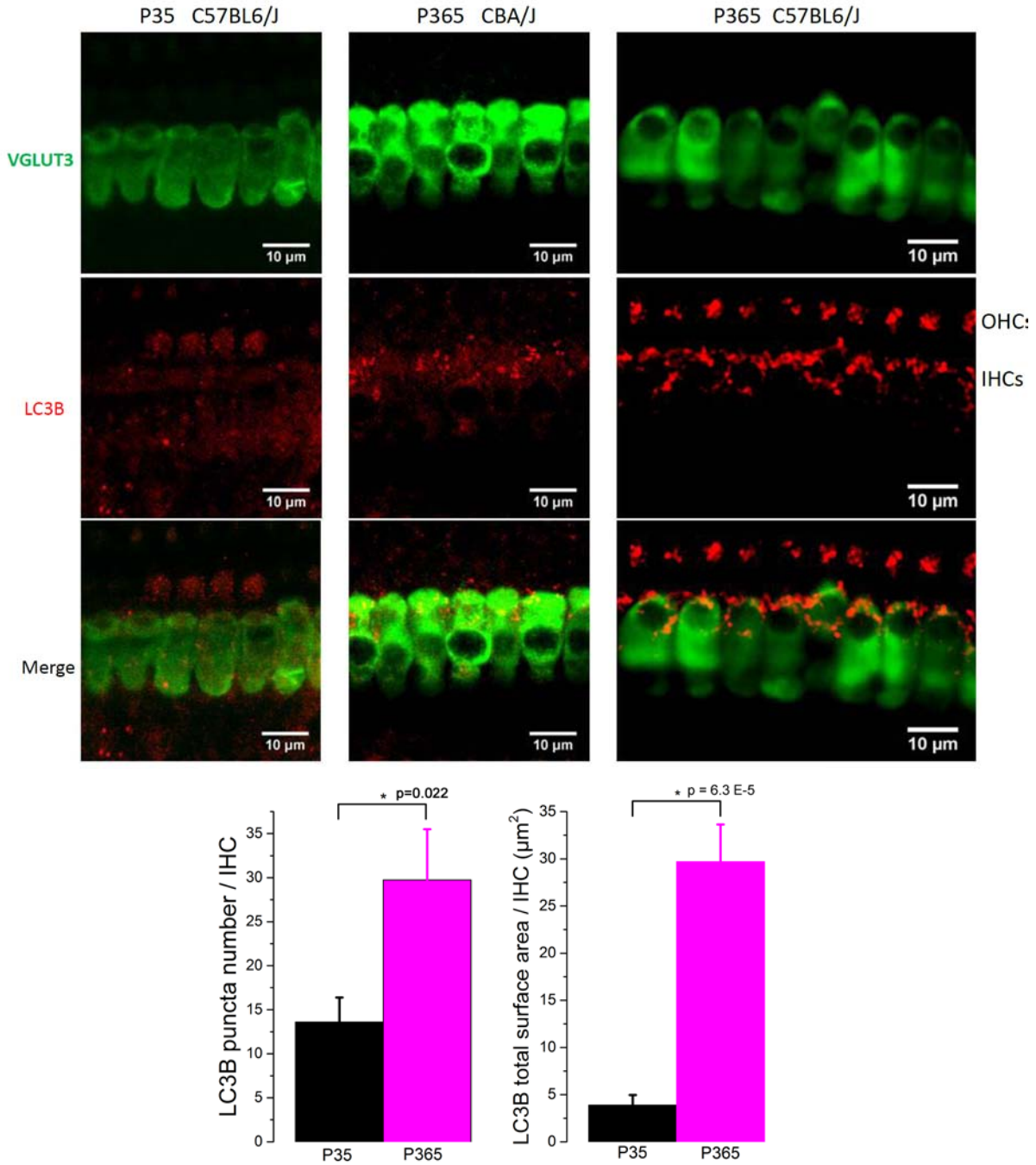

Figure 8: LC3-positive structures are prominent in aging IHCs

Representative confocal immunofluorescence images showing LC3B staining in IHCs from young P30 C57BL/6J (left), old P365 CBA/J (middle) and old P360 C57BL/6J (right) mice. The histograms below show the quantification of the LC3B puncta average number and average mean surface area per IHC. Images were obtained from processing stack images using ImageJ quantification tool (3D-object counter). Quantification was performed from 25 to 30 IHCs for each condition in the mid-cochlea (encoding region 8-16 kHz; 3 mice). Asterisks indicate statistical significance $p < 0.05$ (unpaired t test).

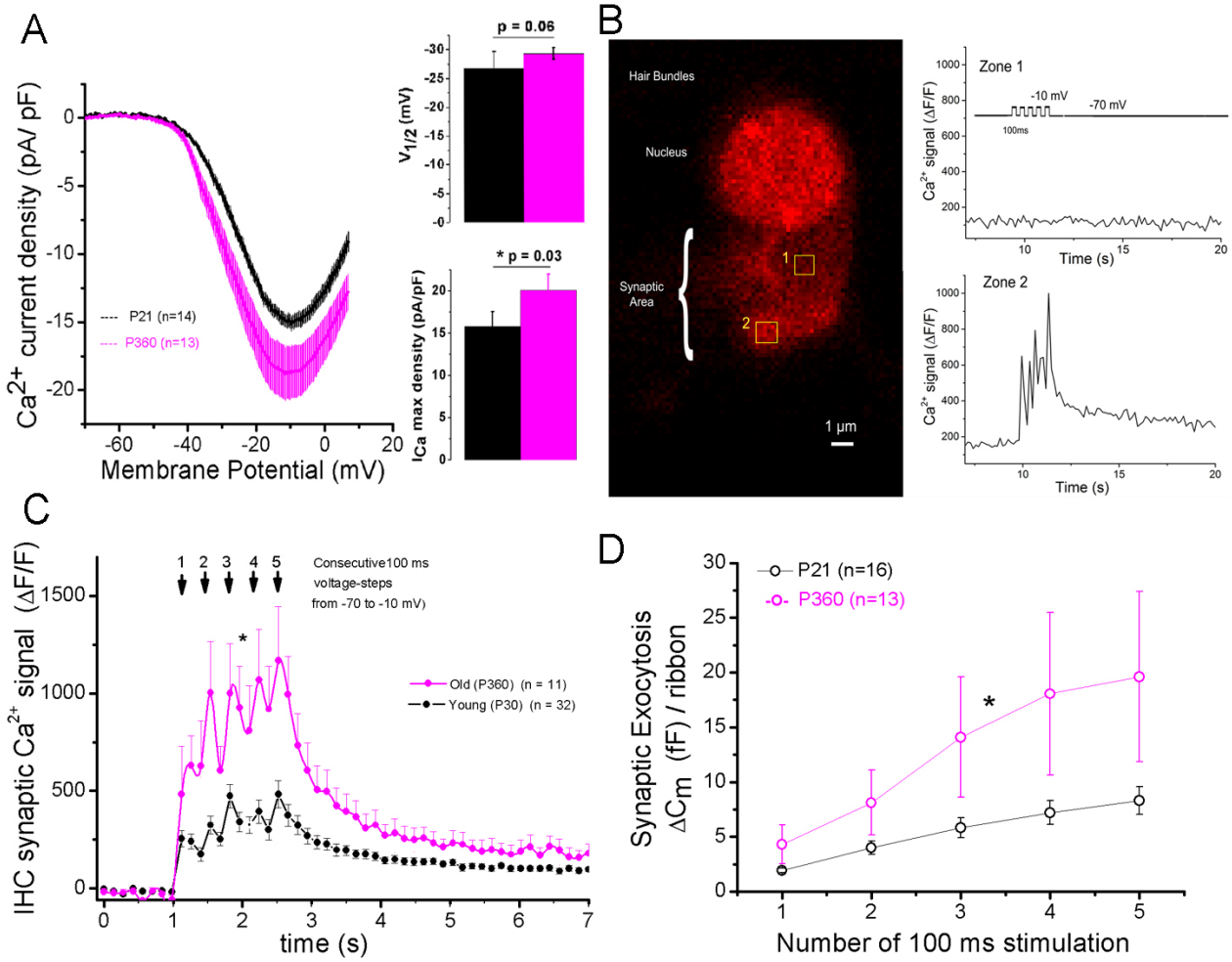

Figure 9: Presynaptic Ca^{2+} signals and exocytosis are exacerbated in IHCs from aged C57BL6/J mice

A) Ca^{2+} current density of old P365 IHCs (pink) was larger as compared to young mature P21 IHCs (black). Under whole-cell patch clamp configuration, IHCs were subjected to a voltage-ramp stimulation from -80 mV to +30 mV in 120 ms, giving a slope change in voltage of 1mV/ms. Asterisks indicate statistical analysis with unpaired two-sample t-test.

B) Example of confocal Ca^{2+} imaging, using the intracellular fluorescent Ca^{2+} indicator Rho-2, in a P365 IHC. The cell was voltage-clamped at -70 mV and stimulated by 5 (100 ms) consecutive voltage-step to -10 mV. The graphs show two examples of fluorescence responses monitored in two square zones (1µm^2) below the cell nucleus, with zone 1 being silent and zone 2 showing five transient Ca^{2+} hot spots (indicating the location of a ribbon active zone).

C) Comparative mean amplitude of transient hot spots showed higher Ca^{2+} responses at the presynaptic active zones of old P365 IHCs (pink) as compared to young mature P30 IHCs (black). Hair cells were depolarized by 5 five consecutive 100 ms depolarizing steps from -70 mV to -10 mV as shown in B. The values n in the graph indicated the number of active zones analyzed for young (6 mice) and old mice (5 mice), respectively.

D) The concomitant Ca^{2+}-induced exocytosis measured during the five 100 ms consecutive stimulations (variation in membrane capacitance normalized to ribbon number or cell size) was larger in old P365 IHCs. The asterisks indicated statistical significant difference with $p<0.05$ (two-way ANOVA, $p = 8.8E-5$; $p = 0.0015$ for graph C and D, respectively) .

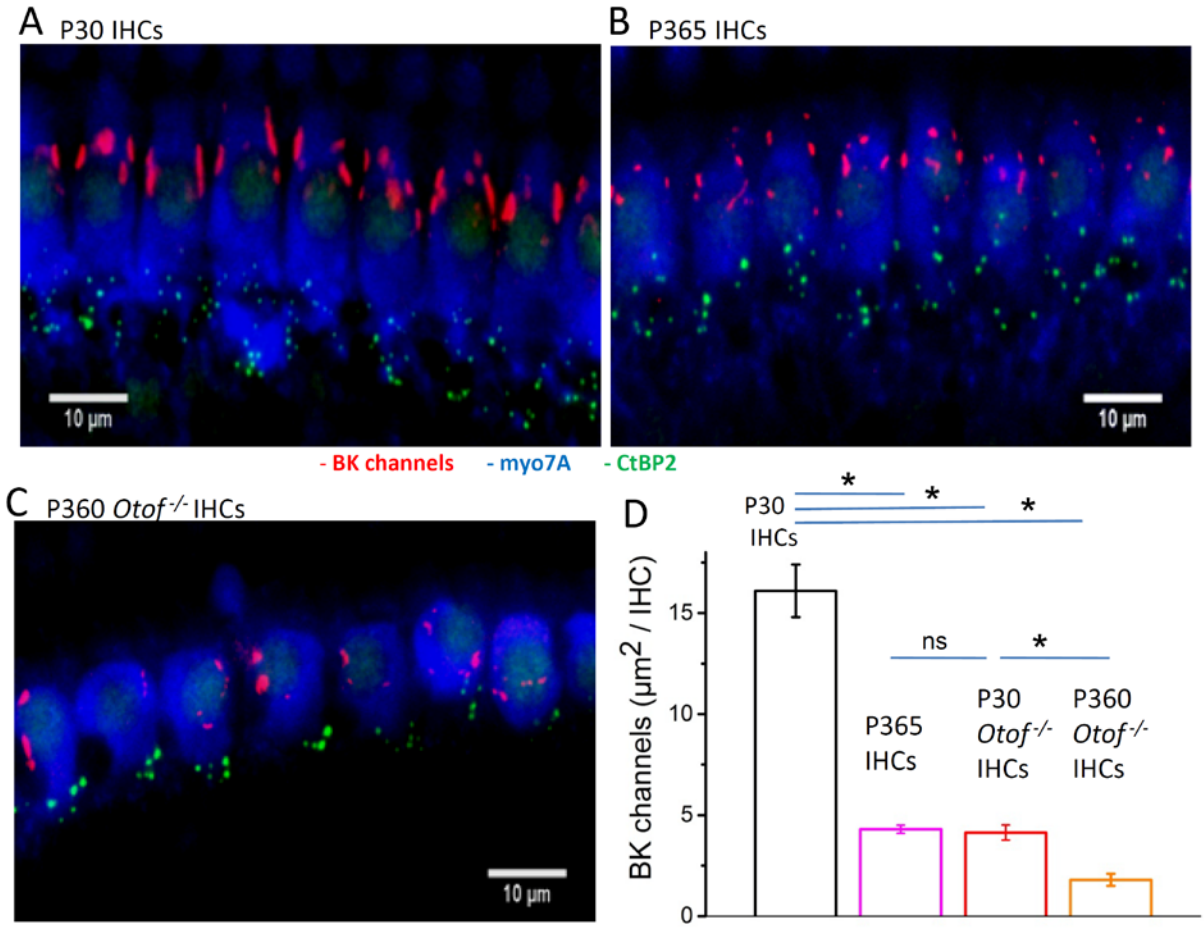

Figure 10: Immunofluorescent confocal imaging of BK channels in aging IHCs

A) Numerous extrasynaptic large BK channel clusters (red) are localized below the cuticular plate of each IHCs in young mature P30 *Otof* $^{+/+}$ C57BL6/J mice.
B) The BK channels clusters are largely reduced in size and number in IHCs of old P365 *Otof*$^{+/+}$ C57BL6/J mice.
C) Few small BK channel clusters were observed in IHCs of P365 *Otof* $^{-/-}$ C57BL6/J mice.
D) Comparative histogram of the total surface area covered by the BK channel clusters per IHC in the mid-turn cochlea (region encoding 8-16 kHz). The number of IHCs analyzed was from left to right: 58; 293; 82; 50. Asterisks indicate statistical significance with $p<0.05$ (from left to right $p = 1.12$ E-7; $p = 1.13$ E-6; $p = 1.13$ E-12; $p = 0.99$; $p = 0.025$; one-way ANOVA post-hocTukey test).

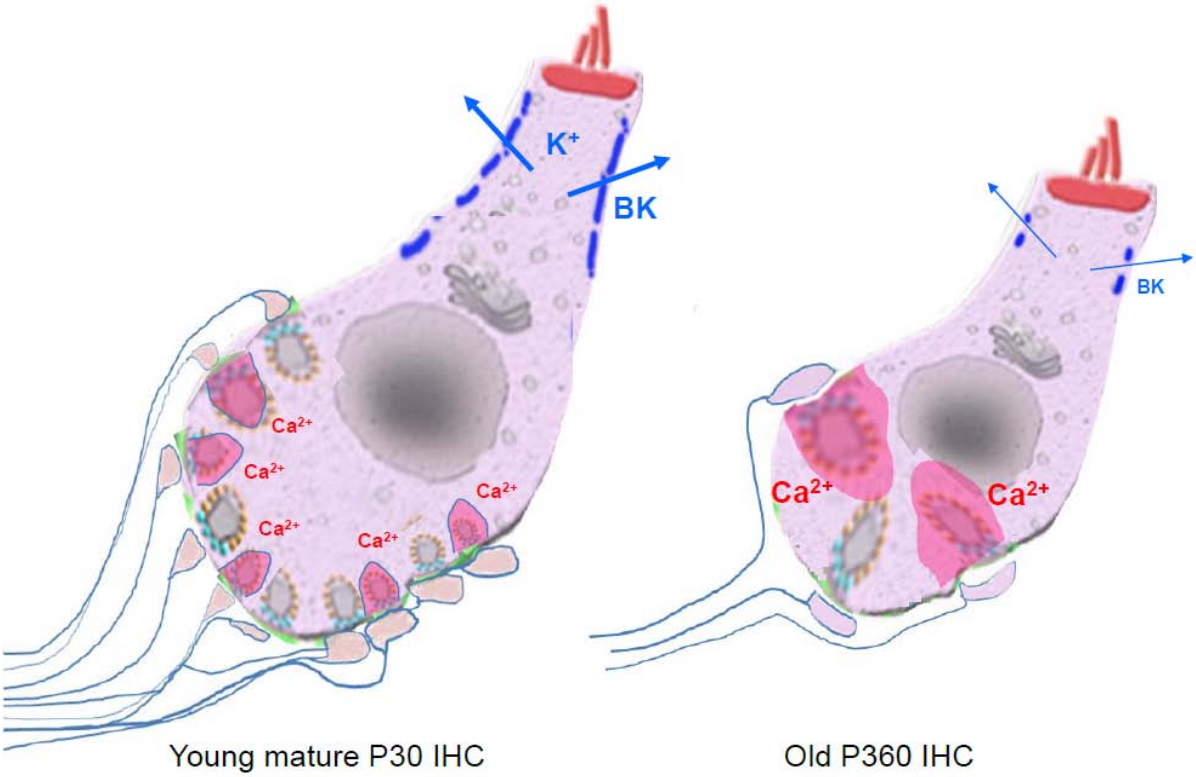

Figure 11: Degeneration of cochlear IHC ribbon synapses in aging C57BL/6J mice
Age-related hearing loss in P360 mice is associated with IHC shrinkage, an important loss of afferent ribbon synapses, a drastic enlargement of the surviving synaptic ribbons, an increase of Ca^{2+} signaling (larger Ca^{2+} microdomain amplitude indicated by larger pink domains around the ribbons) and a large decrease in extrasynaptic BK channel clusters (blue bars). Similar features of synapse alteration were observed in young mature P30 IHCs lacking the Ca^{2+} sensor otoferlin, indicating that the synaptic degenerative process is independent of glutamate exocytosis and excitotoxicity.